The Astrophysical Journal, 964:129 (21pp), 2024 April 1 https://doi.org/10.3847/1538-4357/ad1b52

The Fate of the Interstellar Medium in Early-type Galaxies. III. The Mechanism of Interstellar Medium Removal and the Quenching of Star Formation

Michał J. Michałowski[1,2,3,15], C. Gall[4], J. Hjorth[4], D. T. Frayer[5], A.-L. Tsai[1], K. Rowlands[6,7], T. T. Takeuchi[8,9], A. Leśniewska[1], D. Behrendt[3], N. Bourne[3], D. H. Hughes[10], M. P. Koprowski[11], J. Nadolny[1], O. Ryzhov[1], M. Solar[1], E. Spring[3,12], J. Zavala[13], and P. Bartczak[1,14]

[1] Astronomical Observatory Institute, Faculty of Physics, Adam Mickiewicz University, ul. Słoneczna 36, 60-286 Poznań, Poland; mj.michalowski@gmail.com
[2] TAPIR, Mailcode 350-17, California Institute of Technology, Pasadena, CA 91125, USA
[3] SUPA (Scottish Universities Physics Alliance), Institute for Astronomy, University of Edinburgh, Royal Observatory, Blackford Hill, Edinburgh EH9 3HJ, UK
[4] DARK, Niels Bohr Institute, University of Copenhagen, Jagtvej 128, DK-2200 Copenhagen N, Denmark
[5] National Radio Astronomy Observatory, P.O. Box 2, Green Bank, WV 24944, USA
[6] AURA for ESA, Space Telescope Science Institute, 3700 San Martin Drive, Baltimore, MD 21218, USA
[7] Department of Physics and Astronomy, Johns Hopkins University, Baltimore, MD 21218, USA
[8] Division of Particle and Astrophysical Science, Nagoya University, Furo-Cho, Chikusa-ku, Nagoya 464-8602, Japan
[9] The Research Center for Statistical machine Learning, the Institute of Statistical Mathematics, 10-3 Midori-cho, Tachikawa, Tokyo 190-8562, Japan
[10] Instituto Nacional de Astrofísica, Óptica y Electrónica (INAOE), Aptdo. Postal 51 y 216, 72000 Puebla, Pue., Mexico
[11] Institute of Astronomy, Faculty of Physics, Astronomy and Informatics, Nicolaus Copernicus University, Grudziądzka 5, 87-100 Toruń, Poland
[12] Anton Pannekoek Institute, University of Amsterdam, Science Park 904, NL-1098 XH Amsterdam, The Netherlands
[13] National Astronomical Observatory of Japan, 2-21-1 Osawa, Mitaka, Tokyo 181-8588, Japan
[14] Instituto Universitario de Física Aplicada a las Ciencias y las Tecnologías (IUFACyT), Universidad de Alicante, Ctra. San Vicente del Raspeig, s/n E-03690 San Vicente del Raspeig, Alicante, Spain
Received 2023 April 25; revised 2023 December 8; accepted 2024 January 3; published 2024 March 22

Abstract

Understanding how galaxies quench their star formation is crucial for studies of galaxy evolution. Quenching is related to a decrease of cold gas. In the first paper we showed that the dust removal timescale in early-type galaxies (ETGs) is about 2.5 Gyr. Here we present carbon monoxide and 21 cm hydrogen line observations of these galaxies and measure the timescale of removal of the cold interstellar medium (ISM). We find that all the cold ISM components (dust and molecular and atomic gas) decline at similar rates. This allows us to rule out a wide range of potential ISM-removal mechanisms (including starburst-driven outflows, astration, or a decline in the number of asymptotic giant branch stars), and artificial effects like the stellar mass–age correlation, environmental influence, mergers, and selection bias, leaving ionization by evolved low-mass stars and ionization/outflows by Type Ia supernovae or active galactic nuclei as viable mechanisms. We also provide evidence for an internal origin of the detected ISMs. Moreover, we find that the quenching of star formation in these galaxies cannot be explained by a reduction in the gas amount alone, because the star formation rates (SFRs) decrease faster (on a timescale of about 1.8 Gyr) than the amount of cold gas. Furthermore, the star formation efficiency (SFE) of the ETGs (SFE $\equiv$ SFR/$M_{\rm H_2}$) is lower than that of star-forming galaxies, whereas their gas mass fractions ($f_{\rm H_2} \equiv M_{\rm H_2}/M_*$) are normal. This may be explained by the stabilization of gas against fragmentation, for example due to morphological quenching, turbulence, or magnetic fields.

Unified Astronomy Thesaurus concepts: Early-type galaxies (429); Elliptical galaxies (456); Quenched galaxies (2016); Galaxy quenching (2040); Interstellar medium (847); Post-starburst galaxies (2176); Stellar feedback (1602); Galaxy ages (576); CO line emission (262); H I line emission (690); Cold neutral medium (266); Molecular gas (1073)

1. Introduction

In order to have a full picture of galaxy evolution, we need to understand how galaxies become passive, i.e., how they stop forming stars, the process called quenching. Star formation ceases either when gas is removed from the galaxy or is made unable to form stars. A galaxy can run out of cold gas when it is used for star formation (i.e., astration; Schawinski et al. 2014; Peng et al. 2015). On the other hand, gas can be expelled or ionized by either supernovae (SNe; Dekel & Silk 1986; Ceverino & Klypin 2009; Muratov et al. 2015; Hopkins et al. 2018a; Li et al. 2020) or evolved low-mass stars (Binette et al. 1994; Conroy et al. 2015; Herpich et al. 2018; Hopkins et al. 2018b). Active galactic nuclei (AGNs) have been claimed to be responsible for heating and removing cold gas, and suppressing star formation in more massive galaxies (Di Matteo et al. 2005; Springel et al. 2005a; Fabian 2012; Bluck et al. 2016, 2020b; Cheung et al. 2016; Hopkins et al. 2016; Piotrowska et al. 2022). The bulge of a galaxy may also make the gas resilient against fragmentation, shutting down star formation (i.e., morphological quenching; Martig et al. 2009, 2013; Bluck et al. 2014, 2020a; Bitsakis et al. 2019; Lin et al. 2019; Gensior et al. 2020). A similar effect can result from turbulence and magnetic fields (Padoan & Nordlund 2002; Federrath & Klessen 2012). Finally, gas may be expelled from a galaxy as a result of interactions with other galaxies and mergers (McGee et al. 2011; Bekki 2014; Davies et al. 2015, 2019; Poggianti et al. 2017; Sazonova et al. 2021).

[15] Fulbright Senior Award Fellow.

The existence of gas in many passive galaxies may contradict the interstellar medium (ISM) removal as the only mechanism of quenching. Indeed, atomic and molecular gas and dust have been detected for a fraction of early-type galaxies (ETGs; Davis et al. 2011, 2016, 2019a; Young et al. 2011; Rowlands et al. 2012; Smith et al. 2012; Alatalo et al. 2013, 2015a; di Serego Alighieri et al. 2013; Davis & Bureau 2016; Ashley et al. 2017, 2018, 2019; Zhang et al. 2019; Richtler et al. 2020; Magdis et al. 2021; Donevski et al. 2023) and poststarburst galaxies (French et al. 2015; Rowlands et al. 2015; Alatalo et al. 2016; Suess et al. 2017; Yesuf et al. 2017; Smercina et al. 2018, 2022; Li et al. 2019; Yesuf & Ho 2020; Bezanson et al. 2022; Otter et al. 2022; Wu et al. 2023; Zanella et al. 2023). Small amounts of dense gas, traced by the hydrogen cyanide (HCN) line, in poststarburst galaxies (French et al. 2018b, 2023) may point at the inability of the gas reservoir to collapse and form stars. This may be due to morphological quenching.

The origin of the ISM in ETGs remains unclear. One possibility is that it is of internal origin, e.g., the leftovers from past star formation or released by low-mass stars (Knapp et al. 1992; Rowlands et al. 2012; Michałowski et al. 2019). If gas is brought in from the outside, then the orientation of its rotation is expected to be random with respect to the kinematic axes of the galaxy. However, analyzing the kinematic misalignment of the stellar and gas components in ETGs, Davis & Bureau (2016) found that the paucity of counter-rotating gas disks implies very short gas depletion rates and unrealistically high merger rates (in order to match the gas detection rate which would otherwise be low for short depletion times). Alternatively, a very long gas relaxation timescale must be invoked, which is consistent with cosmological simulations (van de Voort et al. 2015). The alignment of the gas/dust disk and stellar component has also been used to argue against an external origin of the ISM in ETGs (Bassett et al. 2017; Sansom et al. 2019; Richtler et al. 2020). Moreover, Griffith et al. (2019) found that the stellar and gas metallicities of ETGs are similar, suggesting an internal origin of gas. Finally, Babyk et al. (2019) found that the molecular gas mass in ETGs is correlated with their hot gas mass, also suggesting an internal origin. In a similar vein, cold gas in simulated ETGs comes from cooling from the hot halo (Lagos et al. 2014).

The other possibility is an external origin of the ISM. In this scenario the ISM is acquired by ETGs by mergers with gas-rich dwarf galaxies or gas inflows. Davis & Young (2019) found only 7% of ETGs have a lower gas metallicity than stellar metallicity (a clear signature of an external origin for the gas), but given very short enrichment timescale (and hence short visibility of low-metallicity features), they estimated that for at least a third of ETGs the gas is of external origin. Moreover, ETGs with dust lanes contain a cold ISM, which has also been shown to be brought in by minor mergers (Davis et al. 2015). An external source of the ISM has been claimed for around half of ETGs, which have misaligned stellar and gas disks (Davis et al. 2011; Barrera-Ballesteros et al. 2014, 2015; Jin et al. 2016; Bryant et al. 2019). This has also been supported by other works (Young et al. 2014; Cao et al. 2022; Woodrum et al. 2022; Lee et al. 2023). This topic has been investigated in simulations by Lagos et al. (2015), who found that the misalignment of the rotation axes of the gas and stellar components is mostly the consequence of cold gas flows.

This is the third paper in a series in which we analyze ISM removal from ETGs. We use the term ETG for galaxies which are morphologically classified as ellipticals, lenticulars (S0), or early-type spirals (Sa and SBa). In Michałowski et al. (2019; Paper I; M19 hereafter) we presented the decline of dust mass as a function of stellar age, measurement of the dust removal timescale, and the origin of dust in these galaxies. In Leśniewska et al. (2023) and O. Ryzhov et al. (2024, in preparation) we present an expanded analysis of 2000 of these galaxies, allowing us to analyze which galaxy properties influence the dust decline. In Nadolny et al. (2024) we found similar galaxies in simulations, providing a physical insight into the mechanism of this process. The objectives of the present paper are (i) to determine the mechanism of the ISM decline in ETGs and (ii) to constrain the mechanism of quenching.

The paper is structured as follows. In Section 2 we present the ETG sample and in Section 3 we describe our new carbon monoxide (CO) and H I data. Section 4 describes the numerical galaxy evolution model used to interpret the data. We present the results in Section 5. We discuss the implication of the gas removal in ETGs on quenching of star formation in Section 6. In Section 7 we discuss possible mechanisms for this gas removal and in Section 8 we discuss the source of energy needed for this process. We close with a summary of our results in Section 9. We use a cosmological model with $H_0 = 70\,\mathrm{km\,s^{-1}}$ $\mathrm{Mpc^{-1}}$, $\Omega_\Lambda = 0.7$, and $\Omega_m = 0.3$. We also assume a Chabrier (2003) initial mass function (IMF), to which all star formation rates (SFRs) and stellar masses were converted (by dividing by 1.6) if given originally assuming the Salpeter (1955) IMF. Errors are given as 1σ.

2. Sample

As in M19, we use the sample of dusty ETGs from Rowlands et al. (2012). This sample includes all galaxies with elliptical/lenticular morphology and red spirals from the Herschel Astrophysical Terahertz Large Area Survey (H-ATLAS; Eales et al. 2010) ∼14 $\mathrm{deg^2}$ Science Demonstration Field (Ibar et al. 2010; Pascale et al. 2011; Rigby et al. 2011; Smith et al. 2011) that are detected at 250 μm. The specific selection criteria used by Rowlands et al. (2012) are:

1. Set within the H-ATLAS Science Demonstration Field.
2. Matched to an optical Sloan Digital Sky Survey source with a spectroscopic redshift in the range $0.01 < z_{\mathrm{spec}} < 0.32$ within a 10″ radius and with a match reliability greater than 0.8.
3. Herschel 250 μm $>5\sigma$ detection.
4. Visually classified by Rowlands et al. (2012) as early-type (elliptical or S0), or red spiral with near-ultraviolet (NUV) to r-band color of $\mathrm{NUV} - r > 4.5$. The color selection has not been applied to ellipticals or lenticulars.

The sample consists of 61 galaxies, including 42 ellipticals or lenticulars, and 19 red spirals (mostly Sa or SBa). These galaxies will here be referred to as ETGs. Recently, Zhou et al. (2021) found that such red spirals have similar star formation histories as ellipticals, so they are treated collectively. We used the galaxy properties derived by Rowlands et al. (2012) based on the spectral energy distribution (SED) modeling using the data from the Galaxy And Mass Assembly (GAMA) survey (Baldry et al. 2010; Robotham et al. 2010; Driver et al. 2011, 2016; Hill et al. 2011). In order to assess the

Table 1
Observing Log for the IRAM 30 m/EMIR Observations with Integration Times and 225 GHz Atmospheric Opacity

Galaxy	Obs. Date	$t_{\rm int}$ (hr)	$\tau_{225\ \rm GHz}$
J085828.5+003814	2015 Jul 28	0.8	0.50–0.73
J085915.7+002329	2015 Jul 30, Oct 9, 2016 Mar 3	5.6	0.41–0.54, 0.19–0.35, 0.1–0.3
J085946.7−000020	2015 Jul 29, 30	2.4	0.70–0.82, 0.27–0.58
J090038.0+012810	2015 Oct 9, 10	3.6	0.19–0.38, 0.48–0.58
J090234.3+012518	2015 Mar 22, 2016 Mar 4	3.4	0.27–0.32, 0.03–0.57
J090238.7+013253	2016 Mar 6	3.8	0.04–0.27
J090312.4−004509	2015 Oct 10, Nov 18	4.8	0.60–0.73, 0.12–0.22
J090352.0−005353	2015 Mar 22	0.8	0.25–0.38
J090551.5+010752	2015 Nov 19	4.4	0.16–0.29
J090718.9−005210	2015 Nov 22, 2016 Mar 1	4.0	0.13–0.35, 0.10–0.46
J090952.3−003019	2015 Nov 20, 22, 2016 Mar 2	7.6	0.18–0.31, 0.11–0.21, 0.05–0.24
J091205.8+002656	2015 Jul 28	0.6	0.47–0.67
J091448.7−003533	2015 Jul 28	0.8	0.44–0.79

AGN power, we also used the [O III] data from single fiber spectroscopy in the GAMA survey (Gordon et al. 2017).[16] 12 of our galaxies are located within their respective star formation main sequence (M19).

3. Data

We observed the CO and H I lines of 13 galaxies from the sample (nine ellipticals and four red spirals). We randomly selected them to have even coverage of the entire stellar age range. They also cover the entire stellar mass range from $10^{9.7}$ to $10^{11}\ M_\odot$.

3.1. IRAM 30 m/EMIR: CO lines

We performed observations with the IRAM 30 m telescope[17] using the Eight MIxer Receiver[18] (EMIR; Carter et al. 2012). We implemented the wobbler switching mode (with the offset to the reference position of 60″), which provides stable and flat baselines and optimizes the total observing time. We centered one intermediate frequency at the frequency of the CO(1–0) line and the other at the frequency of the CO(2–1) line (the latter was not possible for all sources, see Table 1). We used the Fourier Transform Spectrometers 200 (FTS-200) backend providing 195 kHz spectral resolution and 16 GHz bandwidth in each linear polarization. The observations were divided into 6 minute scans, each consisting of 12 scans 30 s long. The pointing was verified every 1–2 hr on the nearby quasar 0823 +033. The observing log is presented in Table 1. We reduced the data using the Continuum and Line Analysis Single Dish Software (CLASS) package within the Grenoble Image and Line Data Analysis Software[19] (GILDAS; Pety 2005). Each spectrum for a given galaxy was calibrated, and corrected for baseline shape. Then all spectra were averaged.

The IRAM30m/EMIR spectra were binned to $30\ \rm km\ s^{-1}$ channels. A Gaussian was fitted to the binned data, and in the case of detections the 2σ width of the Gaussian was adopted to integrate the line flux. In cases of nondetections, a $[-200, 200]\ \rm km\ s^{-1}$ width was adopted. The error per spectral channel was calculated using the ranges $[-900, -400]\ \rm km\ s^{-1}$ and $[400, 900]\ \rm km\ s^{-1}$. Then the uncertainty of the flux estimation was calculated by a Monte Carlo simulation. We calculated the line luminosities based on Equation (3) in Solomon et al. (1997). The molecular masses were calculated using $\alpha_{\rm CO} = 5\ M_\odot (\rm K\ km\ s^{-1}\ pc^2)^{-1}$ (the conversion includes helium). The choice of the Galactic CO-to-H_2 conversion factor is justified by the fact that most ETGs have solar metallicity (Conroy et al. 2014; Davis & Young 2019). The widths of the lines, integrated fluxes, luminosities, and the resulting molecular gas masses are presented in Table 2. In addition to the results from the CO(1–0) line, the table shows those from the CO(2–1) line if such tuning was possible. The CO spectra are shown in the left and middle columns of Figure A1 in the Appendix. Out of 13 targets for CO(1–0) we detected nine, and out of nine targets for CO(2–1) we detected five.

3.2. GBT: H I Line

We performed observations with the Green Bank Telescope (GBT)[20] using the Versatile GBT Astronomical Spectrometer (VEGAS). We used the mode with 61 kHz spectral resolution (corresponding to $14\ \rm km\ s^{-1}$ at the H I frequency). The observations were divided into scans lasting 3 or 5 minutes. The flux calibration was done using observations of 3C 286, whereas pointing and focus were verified using observations of 0744-0629 (radio source 4C –06.18) every 3 hr. The observing log is presented in Table 3. We used the GBTIDL package[21] to reduce the data. We calibrated each spectrum individually and then averaged them.

We processed the H I GBT/VEGAS spectra in a similar way as for the CO data. The data were not usable for J085934.1 +003629 and J091205.8+002656 due to strong RFI. We calculated the atomic gas masses based on Equation (2) in Devereux & Young (1990). The widths of the lines, integrated fluxes, luminosities, and the resulting atomic gas masses are presented in Table 4. The H I spectra are shown in the right column in Figure A1 in the Appendix. Out of eight targets with usable data we detected seven. The features at $500\ \rm km\ s^{-1}$ for J085828.5+003814 and J090551.5+010752 are likely due to RFI, because they are present only in a fraction of the data.

[16] www.gama-survey.org/dr3/data/cat/SpecLineSFR/
[17] Proposal nos. 198-14, 62-15, and 174-15; PI: M. Michałowski.
[18] www.iram.es/IRAMES/mainWiki/EmirforAstronomers
[19] www.iram.fr/IRAMFR/GILDAS
[20] Proposal nos. 16A-054 and 16B-037; PI: M. Michałowski.
[21] gbtidl.nrao.edu

Table 2
CO Fluxes and Luminosities from the IRAM 30 m/EMIR Observations

Galaxy	CO(1–0)				CO(2–1)			
	FWHM (km s^{-1})	$F_{\rm int}$ (Jy km s^{-1})	L' (10^8 K km s^{-1} pc^2)	$M_{\rm H_2}$ (10^8 $M_\odot$)	FWHM (km s^{-1})	$F_{\rm int}$ (Jy km s^{-1})	L' (10^8 K km s^{-1} pc^2)	$M_{\rm H_2}$ (10^8 $M_\odot$)
J091205.8+002656	158 ± 20	10.46 ± 1.38	14.32 ± 1.89	71.6 ± 9.5	226 ± 12	19.41 ± 3.37	6.64 ± 1.15	66.4 ± 11.5
J091448.7-003533	268 ± 22	6.94 ± 1.32	9.31 ± 1.76	46.5 ± 8.8	194 ± 71	5.59 ± 2.70	1.87 ± 0.91	18.7 ± 9.1
J085828.5+003814	235 ± 16	6.17 ± 1.15	7.79 ± 1.45	39.0 ± 7.2	⋯	9.48 ± 3.95	<5.49	<54.9
J085946.7-000020	⋯	0.60 ± 0.74	<2.67	<13.3	⋯	0.87 ± 1.12	<1.00	<10.0
J085915.7+002329	⋯	0.01 ± 0.52	<0.06	<0.3	⋯	⋯	⋯	⋯
J090038.0+012810	235 ± 10	4.33 ± 0.45	5.44 ± 0.57	27.2 ± 2.8	225 ± 28	4.84 ± 0.71	1.52 ± 0.22	15.2 ± 2.2
J090312.4-004509	⋯	0.40 ± 0.39	<1.27	<6.4	⋯	0.39 ± 0.42	<0.33	<3.3
J090551.5+010752	⋯	0.45 ± 0.34	<1.42	<7.1	⋯	1.12 ± 0.63	<0.75	<7.5
J090952.3-003019	237 ± 56	1.36 ± 0.27	1.46 ± 0.29	7.3 ± 1.4	235 ± 22	2.68 ± 0.39	0.72 ± 0.11	7.2 ± 1.1
J090718.9-005210	242 ± 18	2.19 ± 0.32	3.46 ± 0.51	17.3 ± 2.6	168 ± 19	2.12 ± 0.69	0.84 ± 0.27	8.4 ± 2.7
J090352.0-005353	427 ± 60	7.26 ± 0.81	36.10 ± 4.04	180.5 ± 20.2	⋯	⋯	⋯	⋯
J090234.3+012518	302 ± 10	1.83 ± 0.52	11.59 ± 3.32	58.0 ± 16.6	⋯	⋯	⋯	⋯
J090238.7+013253	254 ± 16	3.13 ± 0.33	19.97 ± 2.09	99.9 ± 10.5	⋯	⋯	⋯	⋯

Note. The columns show the Gaussian FWHM of the line, the integrated line flux within the dotted lines in Figure A1, the line luminosity, and the molecular gas mass assuming $\alpha_{\rm CO} = 5\ M_\odot$(K km s^{-1} pc^2)$^{-1}$. The left set is for CO(1–0) and the right set is CO(2–1) for galaxies for which simultaneous setting for this line was possible.

4. Numerical Model

To aid the interpretation of the observed data we use the chemical dust evolution model from Gall et al. (2011a; hereafter GAH11), allowing us to follow the dust and gas removal with stellar age. The model considers SN and asymptotic giant branch (AGB) star dust production at different efficiencies (Gall et al. 2011b, 2011c). It assumes that all material is recycled, and hence available for star formation, instantaneously after the deaths of the stars. Furthermore, ISM dust destruction through SN shocks is either turned off or set at a moderate rate. We calculate a suite of models for which we either switch on or off the SN and AGB star dust and gas recycling. Additionally we investigate gas and dust removal through outflows.

The evolution of dust and gas in a galaxy is:

$$\frac{dM_{\rm d}(t)}{dt} = E_{\rm d,SN}(t) + E_{\rm d,AGB}(t) - \eta_{\rm d}(t)\,(\psi(t) + \xi_{\rm SN}(t) + \zeta_{\rm out}(t)), \quad (1)$$

and:

$$\frac{dM_{\rm g}(t)}{dt} = E_{\rm g,SN}(t) + E_{\rm g,AGB}(t) + \eta_{\rm d}(t)\,\xi_{\rm SN}(t) - (1 - \eta_{\rm d}(t))\,(\psi(t) + \zeta_{\rm out}(t)). \quad (2)$$

Here, $E_{\rm d,SN}(t)$ and $E_{\rm d,AGB}(t)$ are, respectively, the SN and AGB dust production (injection) rates as defined in GAH11 while $E_{\rm g,SN}(t)$ and $E_{\rm g,AGB}(t)$ are the corresponding rates for the recycled gas phase elements (Equation (6) in GAH11). The variable $\eta_{\rm d}(t) = M_{\rm d}(t)/M_{\rm ISM}(t)$ can be understood as the "dust-to-gas mass ratio," or the fraction of dust present in the ISM. The evolution of the SFR, $\psi(t)$, here is chosen to represent the measured SFRs (Figure 1 in M19 and Equation (8) below) as:

$$\psi(t) = \psi_{\rm ini}\ e^{-\,a(t)},\ a(t) = \frac{T_{\rm gal}(t)}{\tau_{\rm SFR}}, \quad (3)$$

where $\psi_{\rm ini}$ is the initial SFR, $T_{\rm gal}(t)$ is the age of the galaxy, and $\tau_{\rm SFR} = 1.8$ Gyr is the star formation decline timescale (duration of the star formation episode). We note that this SFR evolution is not coupled to the total amount of gas in the galaxy as it would be by a Schmidt–Kennicutt law (Kennicutt 1998) and as defined in GAH11. Instead, the formulation here is based on the observations (Figure 1 in M19) of the galaxies in question.

Table 3
Observing Log for the GBT/VEGAS Observations

Galaxy	Obs. Date	$t_{\rm int}$ (hr)
J085828.5+003814	2016 Apr 19, Jul 17, 31, Oct 22	10.5
J085915.7+002329	2016 Mar 20	3.2
J085946.7−000020	2016 Apr 23, 24, Nov 14, Dec 1	10.2
J090038.0+012810	2016 Apr 20, Oct 19	6.1
J090312.4−004509	2016 Apr 24, 25, Oct 23	7.4
J090551.5+010752	2016 Mar 21, Jul 16, Oct 18, Nov 19	8.3
J091205.8+002656	2016 Nov 20, 27	3.5[a]
J091448.7−003533	2016 Mar 12, Oct 23, Nov 29	7.2
J085934.1+003629	2015 Apr 18	1.8[a]
J091051.1+020121	2016 Mar 19, 20, Nov 1, Dec 1	7.4

Note.
[a] The data were not usable due to strong radio-frequency interference (RFI).

An additional cold gas removal is considered, either in a form of gas heating or physical ISM removal. It is modeled as:

$$\zeta_{\rm out}(t) = \frac{M_{\rm ISM,out}}{\tau_{\rm ISM}}\ e^{-\,b(t)},\ b(t) = \frac{T_{\rm gal}(t)}{\tau_{\rm ISM}}, \quad (4)$$

where $M_{\rm ISM,out}$ is the amount of ISM material removed over timescale $\tau_{\rm ISM}$.

The variable $\xi_{\rm SN}(t) = M_{\rm cl}\,R_{\rm SN}(t)$ defines how much ISM mass, $M_{\rm cl}$, is completely cleared of dust by core-collapse supernovae (CCSNe; Dwek et al. 2007), with $R_{\rm SN}(t)$ being the CCSN rate. We have been testing zero to moderate dust destruction with an $M_{\rm cl}$ of 0, 50, 100, or 500 $M_\odot$. Both the CCSNe rate and AGB rate are calculated as:

$$R_{\rm AGB,SN}(t) = \int_{m_{\rm L(AGB,SN)}}^{m_{\rm U(AGB,SN)}} \psi(t-\tau)\,\phi(m)\,dm, \quad (5)$$

Table 4
H I Fluxes and Luminosities from the GBT/VEGAS Observations

Galaxy	FWHM (km s^{-1})	$F_{\rm int}$ (Jy km s^{-1})	L' (10^{10} K km s^{-1} pc^2)	$M_{\rm H\,I}$ (10^8 $M_\odot$)
J085828.5+003814	243 ± 15	0.674 ± 0.062	56.12 ± 5.16	86.52 ± 7.95
J085915.7+002329	188 ± 2	1.960 ± 0.038	7.44 ± 0.14	11.02 ± 0.21
J085946.7-000020	464 ± 9	1.377 ± 0.044	116.47 ± 3.69	179.64 ± 5.69
J090038.0+012810	233 ± 15	0.460 ± 0.042	38.08 ± 3.44	58.71 ± 5.30
J090312.4-004509	322 ± 13	0.390 ± 0.030	27.63 ± 2.11	42.43 ± 3.25
J090551.5+010752	···	0.169 ± 0.041	<20.83	<32.11
J091051.1+020121	173 ± 11	0.377 ± 0.054	34.20 ± 4.87	52.84 ± 7.52
J091448.7-003533	398 ± 26	0.587 ± 0.048	51.85 ± 4.28	80.05 ± 6.61

Note. The columns show the Gaussian FWHM of the line, the integrated line flux within the dotted lines on Figure A1, the line luminosity, and the atomic gas mass.

which assumes that only single stars form. $R_{\rm AGB,SN}(t)$ is regulated by the IMF, $\phi(m)$, and $\psi(t-\tau)$ is the lifetime of a star with given zero-age main-sequence mass m. The model parameters are summarized in Table A1.

5. Results

Our aim is to investigate the time evolution of various galaxy properties, using the stellar age as a time proxy, so first we verify that indeed the ages of these galaxies increase linearly with time. In principle this is not the case for all galaxies, especially for highly star-forming ones for which the mean stellar age may even decrease with time. Strictly speaking the stellar age increases linearly with time when the SFR is zero. Our galaxies have very low levels of star formation and large stellar masses, so they should be close to this approximation, because the mean stellar age is not affected significantly by the presence of new populations of stars and therefore should grow linearly with time.

We checked the age evolution with time using 2000 simulated analogs of our galaxies selected in a very similar way: a similar redshift distribution and similar stellar masses and dust masses, so that the 250 μm flux would be detectable as for the early-type morphological classification of the real sample, and low star formation activity placing them below the main sequence (Nadolny et al. 2024). These are Millennium Simulations with LGalaxies semianalytical models with $\sim 100^3$ Mpc^3 boxes (Springel et al. 2005b; Lemson & the Virgo Consortium 2006; Henriques et al. 2020). Unlike for observed galaxies, for each of the simulated galaxies we have complete knowledge of the light-weighted stellar age as a function of the age of the Universe (cosmic time).

In order to analyze the time evolution of the ages for the entire sample, we need to choose a common time zero-point. Galaxies observed at similar ages of the Universe have a range of stellar ages, so in order to assess how the stellar ages evolve with time for the entire sample, we shifted horizontally (in time) the age–time tracks, so that at the time of observation, the cosmic time is equal to the measured stellar age. With such a choice of the time zero-point, galaxies with higher levels of current star formation activity than in the past should be located below the age = time line (i.e., their ages are lower than the cosmic time value) due to a significant number of young stars. On the other hand, galaxies with long periods of a constant SFR should be located above this line (i.e., their ages are higher than the cosmic time value), because their mean stellar age does not change in time.

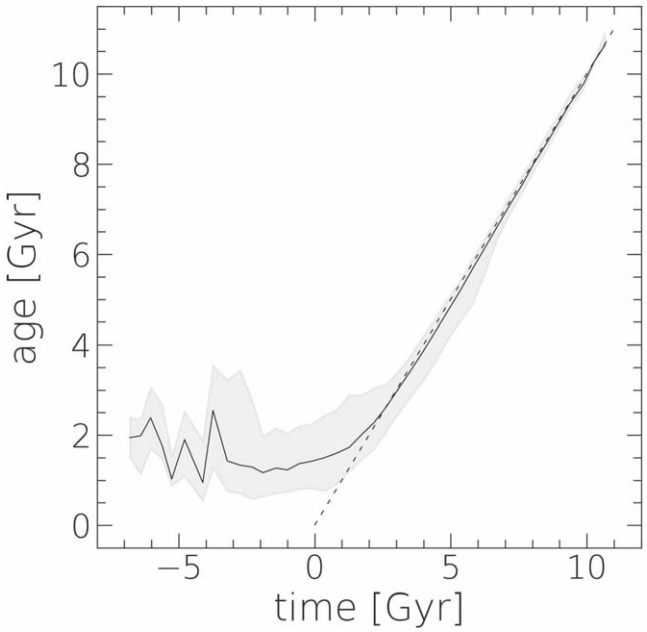

Figure 1. Light-weighted stellar age as a function of cosmic time for simulated dusty ETGs (Nadolny et al. 2024). The black solid line is the running average for given time, whereas the gray shaded region represents the 1σ range. The dashed line indicates the linear evolution when the stellar age is equal to the value of cosmic time. The time reaches negative values because of how the moment when time is equal zero was set, in order to have the time equal to the stellar age at the moment of observation. This figure shows that the stellar ages increase linearly with time for dusty ETGs, so can be used as a time proxy.

Figure 1 shows the age–time evolution for the simulated dusty ETGs. It is clear that neither of the nonlinear scenarios described above applies to them. Their mean stellar ages increase linearly with time at least during the last 8 Gyr, which is the range of interest of our study. Very low scatter around the age = time line indicates that very few galaxies exhibit levels of star formation strong enough to break the linearity of stellar age with time.

Having demonstrated that the stellar ages of dusty ETGs increase linearly with time, at least for the dusty ETGs selected in the way we do here, we come back to the observed sample. In order to compare galaxies with different masses, we normalize the gas and dust masses by their stellar masses. We show the molecular and atomic gas-to-stellar mass ratios ($M_{\rm H_2}/M_*$ and $M_{\rm H\,I}/M_*$) as a function of stellar age in Figure 2. We detect a decline of the gas-to-stellar mass ratios with age, similar to the evolution of the dust-to-stellar ratio ($M_{\rm dust}/M_*$) from M19 and Leśniewska et al. (2023). For the $M_{\rm H_2}/M_*$–age and $M_{\rm H\,I}/M_*$–

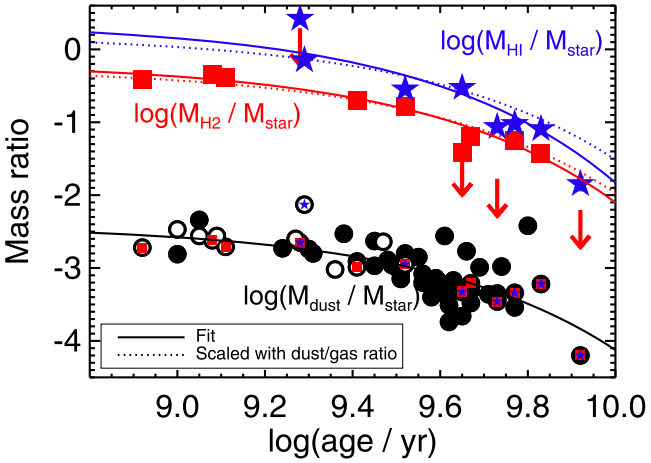

Figure 2. Ratios of molecular (large red squares and arrows for upper limits), atomic (large blue stars) gas, and dust (black circles; M19) mass to stellar mass as a function of luminosity-weighted stellar age of the ETGs galaxies detected by Herschel from the sample of Rowlands et al. (2012). The exponential fits to the gas-to-stellar and dust-to-stellar mass ratios (Equations (6) and (7)) are shown as solid lines, colored the same as the data points. The red and blue dotted lines denote the curves for the dust-to-stellar ratio shifted upwards by the measured average gas-to-dust ratios of $\log(M_{\rm H_2}/M_{\rm dust}) = 2.144 \pm 0.018$ and $\log(M_{\rm H\,I}/M_{\rm dust}) = 2.610 \pm 0.011$. Small red squares and blue stars mark the galaxies which we observed at CO and H I, respectively. Open circles denote galaxies which are within the main sequence (see Figure 1 in M19). All ISM components decline at a similar rate.

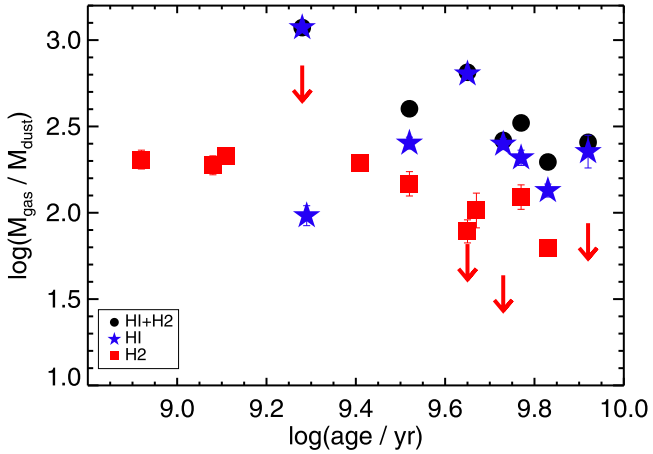

Figure 3. Gas-to-dust ratios as a function of luminosity-weighted stellar age. Red squares, blue stars, and black circles denote molecular gas, atomic gas, and total gas, respectively (the latter only for galaxies with both CO and H I measurements). Only very weak trends are present, indicating that the ISM components are affected by the same mechanism.

age diagrams the Spearman's rank correlation coefficients are −0.9 and the probabilities of the null hypothesis of no correlation are 0.00094 (3.3σ) and 0.019 (2.3σ), respectively. Due to a smaller sample size, this significance is lower than the 5.5σ we reported for the correlation between $M_{\rm dust}/M_*$ and age (probability of 4×10^{-11}; M19).

Figure 2 presents the decline of ISM mass as a function of age. We fitted an exponential function to the gas-to-stellar mass ratios and obtained:

$$\log(M_{\rm H_2}/M_*) = (-{\rm age/Gyr})/(5.21 \pm 0.24) - (0.18 \pm 0.03),$$
$$\log(M_{\rm H\,I}/M_*) = (-{\rm age/Gyr})/(4.54 \pm 0.23) + (0.37 \pm 0.05). \quad (6)$$

This corresponds to the characteristic exponential timescale of gas removal of $\tau_{\rm H_2} = 2.26 \pm 0.11$ Gyr and $\tau_{\rm H\,I} = 1.97 \pm 0.10$ Gyr (half-life times of $t_{1/2\,\rm H_2} = \tau_{\rm H_2} \ln 2 = 1.57 \pm 0.07$ Gyr and $t_{1/2\,\rm H\,I} = 1.37 \pm 0.07$ Gyr). The gas removal timescales are consistent with the dust removal timescales (at 2σ) we measured in M19 and Leśniewska et al. (2023), where we obtained the characteristic exponential timescale of dust removal to be $\tau_{\rm dust} = 2.53 \pm 0.17$ and 2.26 ± 0.18 Gyr, respectively (half-life time of 1.75 ± 0.12 and 1.57 ± 0.12 Gyr, respectively).

The decline of the gas amount in ETGs with time is seen in models (Calura et al. 2017), but has not been measured directly before. On the other hand, Smercina et al. (2018) detected a dust decline with age for poststarburst galaxies with ages up to 1 Gyr, and a very weak gas decline. They interpret this as the effect of sputtering of dust grains in hot gas. With a larger sample of poststarburst galaxies, French et al. (2018a) detected a gas decline on the timescale of 100–200 Myr. Similarly, molecular gas was found in poststarburst galaxies at $z \sim 0.6$ only for those which were quenched less than 150 Myr ago, indicating rapid gas removal (Bezanson et al. 2022). The timescale we measure is comparable to that inferred by Gobat et al. (2020), based on the low gas fraction of low-z ETGs, and higher than the quenching timescale due to environmental influence (Gobat et al. 2015).

The weighted averages of the gas-to-dust ratios are $\log(M_{\rm H_2}/M_{\rm dust}) = 2.144 \pm 0.018$ and $\log(M_{\rm H\,I}/M_{\rm dust}) = 2.610 \pm 0.011$. In Figure 2 we used these averages to scale up the exponential fit to the dust-to-stellar ratios (M19):

$$\log(M_{\rm dust}/M_*) = (-{\rm age/Gyr})/(5.8 \pm 0.4) - (2.41 \pm 0.09). \quad (7)$$

Indeed the evolution of the gas-to-stellar ratios are consistent with these scaled curves.

The gas-to-dust ratios are either independent of or weakly decline with age (Figure 3). There is a hint of a decline of the $M_{\rm H_2}/M_{\rm dust}$ ratio with age at the $\sim 2.9\sigma$ level (probability of the null hypothesis of no correlation is 0.0037 and a Spearman's rank correlation coefficient of −0.85). There is no indication of the decline of the $M_{\rm H\,I}/M_{\rm dust}$ ratio (a Spearman's rank correlation coefficient of −0.09 and the probability of the null hypothesis is 0.87). We note that the gas-to-dust ratios we found are similar to those of star-forming galaxies. Hence, these ETGs do not belong to the class of passive galaxies at $0 < z < 3$ with extremely high ratios, recently identified in simulations (Whitaker et al. 2021; Donevski et al. 2023).

The ETGs in our sample follow the evolutionary sequence found for other galaxies based on ISM properties. In Figure 4 we show the dust-to-baryon mass ratio $[M_{\rm dust}/(M_* + M_{\rm H\,I})]$ as a function of atomic gas fraction $[M_{\rm H\,I}/(M_* + M_{\rm H\,I})]$ together with dust-selected galaxies (Clark et al. 2015). Modeling shows that galaxies evolve from the left (high gas fractions) to the right (low gas fractions), increasing their dust-to-baryon ratios initially and then following a decline (Clark et al. 2015; De Vis et al. 2017a, 2017b, 2019; Donevski et al. 2020; Nanni et al. 2020). The ETGs in our sample have low gas fractions, consistent with being among the oldest galaxies in this plot. The only galaxy with a high gas fraction is J085915.7 +002329, which has the lowest stellar mass in our sample $[\log(M_*/M_\odot) = 8.62]$. It is indeed one of the youngest as well, with an age of $10^{9.3}$ yr.

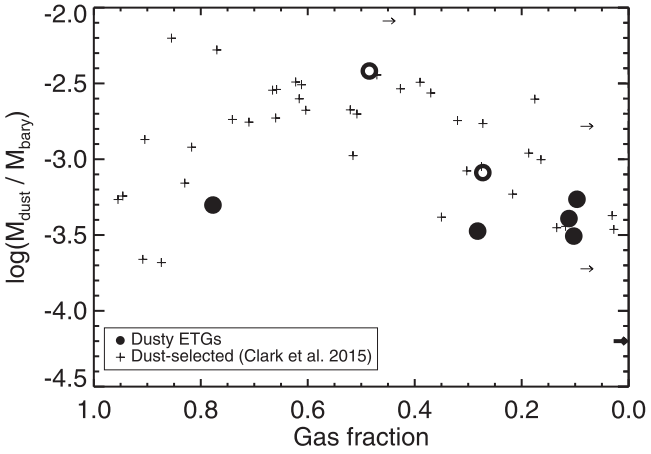

Figure 4. Dust-to-baryon mass ratio $[M_{\rm dust}/(M_* + M_{\rm H\,I})]$ as a function of atomic gas fraction $[M_{\rm H\,I}/(M_* + M_{\rm H\,I})]$ of the ETGs in our sample (large black circles and the thick arrow) compared with the dust-selected galaxies from Clark et al. (2015; plus signs and thin arrows). Open circles denote galaxies which are within the main sequence (see Figure 1 in M19). The ETGs in our sample are located in the low-gas-fraction regime, expected for old galaxies.

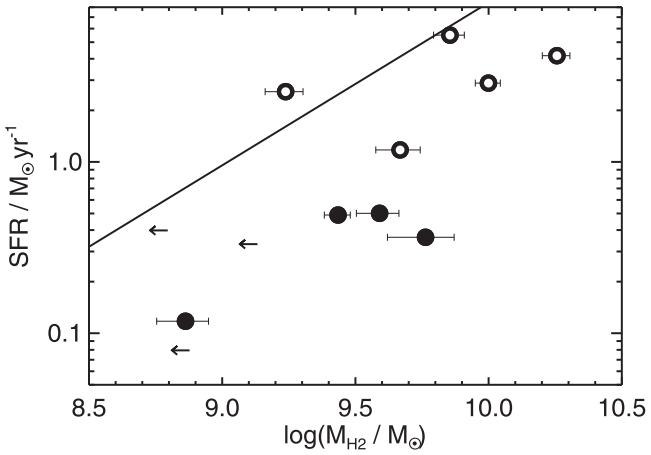

Figure 5. SFR as a function of molecular gas mass. Arrows denote upper limits. Open circles denote galaxies which are within the main sequence (see Figure 1 in M19). The solid line denotes the relation for star-forming galaxies (Equation (1) in Michałowski et al. 2018). The ETGs are below the relation for star-forming galaxies, indicating that their gas reservoirs are ceasing to be able to form stars.

The SFRs of the ETGs in our sample decline faster than the masses of their ISMs, as noted in Hjorth et al. (2014). The exponential fit of M19 (their Figure 1) results in:

$$\log({\rm SFR}) = (-{\rm age/Gyr})/(4.0 \pm 0.4) + (0.57 \pm 0.09), \quad (8)$$

which corresponds to the characteristic exponential time $\tau_{\rm SFR} = 1.8 \pm 0.4$ Gyr or half-life time $t_{1/2,{\rm SFR}} = 1.22 \pm 0.28$ Gyr. This is ∼40% faster than the dust decline (Equation (7)).

We note that the exponential decline parameterization for the SFR in the above equation and in the model (Equation (3)) is justified for these old galaxies. First, this function fits the data (Figure 1 of M19). Second, the SED fits from Rowlands et al. (2012) resulted in no recent starbursts in this sample, with the time since the last starburst being >500 Myr for all galaxies, >1 Gyr for 80% of the sample, and >2 Gyr for 56% of the sample. The existence of these bursts does not affect our analysis because in Equation (8) we quantify the evolution of the average SFR after these episodes. Similarly, the assumption

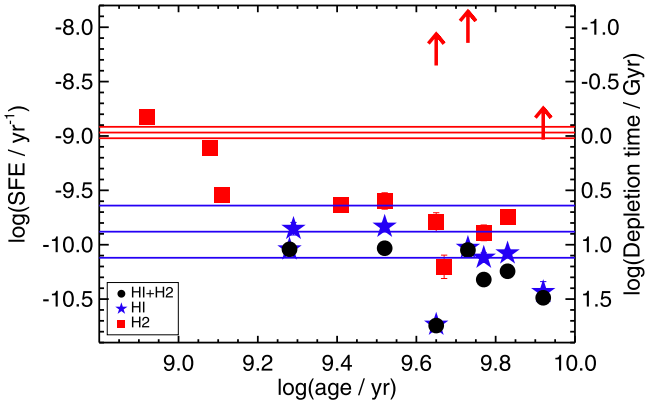

Figure 6. SFE ($\equiv$SFR$/M_{\rm gas}$) as a function of luminosity-weighted stellar age. Red squares, blue stars, and black circles denote molecular gas, atomic gas, and total gas, respectively (the latter only for galaxies with both CO and H I measurements). The solid lines represent the SFEs of star-forming galaxies with SFR = 0.01, 0.1, and 1 $M_\odot$ yr^{-1} (from bottom to top) using Equation (1) in Michałowski et al. (2015; atomic gas) and Equation (1) in Michałowski et al. (2018; molecular gas) colored in the same way as the data points. The molecular SFEs decline with age and are lower than those of the star-forming galaxies, whereas the atomic SFEs stay consistent with those of the star-forming galaxies.

of the exponential decline of the SFR in the model has almost no impact on the resulting properties, because the SFRs are low, so the astration is weak, independent of what parameterization is adopted, as long as it is consistent with the low measured values.

The galaxies in our sample have low SFRs for their molecular gas masses, as demonstrated in Figure 5. They are below the Schmidt–Kennicutt law by a factor of several.

Hence, the star formation efficiencies (SFE $\equiv$ SFR$/M_{\rm gas}$) of our sample are low with a mean value of $\log({\rm SFE/yr^{-1}}) \sim -9.6$, -10.2, and -10.3 (depletion times $1/{\rm SFE} \sim 4$, 16, and 20 Gyr), using the molecular, atomic, and total gas mass, respectively (Figure 6). These efficiencies are similarly low as for the sample of ETGs with dust lanes (Davis et al. 2015) and some poststarburst galaxies (Alatalo et al. 2015b; French et al. 2015, 2023; Rowlands et al. 2015; Smercina et al. 2018, 2022; Bezanson et al. 2022; Luo et al. 2022); at the lower limit for high-z ETGs (Magdis et al. 2021); and lower than the full ETG ATLAS$^{\rm 3D}$ sample (Davis et al. 2014; Kokusho et al. 2017). In Figure 6 we compare the SFEs of our sample with those of the general star formation population. For the molecular and atomic gas we used Equation (1) of Michałowski et al. (2018) and Equation (1) of Michałowski et al. (2015), respectively (see similar estimates in Sargent et al. 2014; Saintonge et al. 2017; Liu et al. 2019; Magdis et al. 2021). Again, the molecular SFEs of galaxies in our sample are lower than those of the star-forming galaxies. The difference is stronger for older ages, so these galaxies keep decreasing their efficiency with time. However, the atomic SFEs are similar to those of star-forming galaxies. This could be because the atomic gas in ETGs is only indirectly connected with star formation.

6. ISM Removal and Quenching

We have provided a measurement of the timescale of ISM removal in ETGs of ∼2.3 Gyr (Equation (6)). This slow ISM removal suggests that either quenching in these galaxies is a slow process or that the main reason for quenching is not exhaustion of the gas supply, but rather gas stabilization that

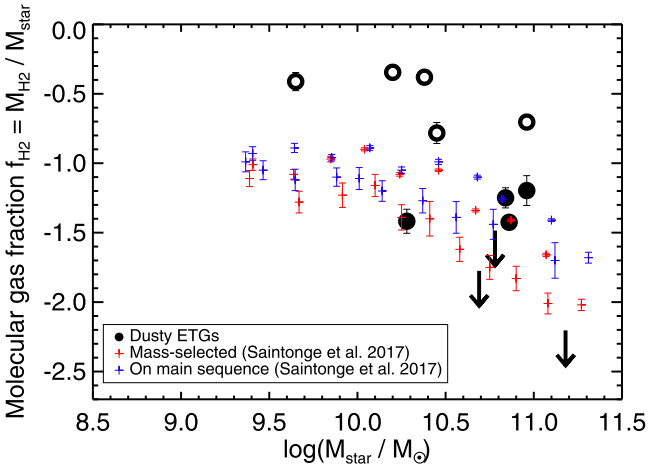

Figure 7. Molecular gas fraction ($f_{H_2} \equiv M_{H_2}/M_*$) as a function of stellar mass for the ETGs in our sample (black circles and arrows). Open circles denote galaxies which are within the main sequence (see Figure 1 in M19). The red and blue symbols correspond to the averages for mass-selected galaxies and only those on the main sequence, respectively (Saintonge et al. 2017). The gas fractions of the ETGs are comparable or higher than those of star-forming galaxies, indicating that the ETGs do not stop forming stars due to lack of gas.

prevents further star formation. Indeed, we have measured a slow SFR decline (Equation (8)). Similarly, the timescale of quenching was measured to be of the order of several gigayears in observed (Peng et al. 2015; Trussler et al. 2020; Kipper et al. 2021; Noirot et al. 2022; Tacchella et al. 2022; Bravo et al. 2023; Donevski et al. 2023) and simulated (Trayford et al. 2016; Nelson et al. 2018; Wright et al. 2019; Park et al. 2022; Walters et al. 2022; Nadolny et al. 2024) galaxies, with the exception of cluster members in which it is shorter (Muzzin et al. 2014; Socolovsky et al. 2018; Davis et al. 2019b; Zavala et al. 2019).

As detailed below, the galaxies in our sample are shutting down their star formation not only because they are running out of gas, but because their SFRs decline faster than the gas amount and they have low SFEs and normal gas fractions.

Even in samples of postmerger and poststarburst galaxies the gas supply was actually higher than in other galaxies with similar masses (French et al. 2015; Rowlands et al. 2015; Alatalo et al. 2016; Suess et al. 2017; Ellison et al. 2018), so quenching in these galaxies is likely related to turbulence, not the exhaustion or expulsion of gas. Morphological quenching, the influence of the bulge making the gas resilient against fragmentation (Martig et al. 2009, 2013; Bluck et al. 2014, 2020a; Bitsakis et al. 2019; Lin et al. 2019; Gensior et al. 2020), or the influence of turbulence and magnetic fields (Padoan & Nordlund 2002; Federrath & Klessen 2012) can also be responsible for the decreasing SFRs. Indeed the galaxies in our sample evolve upwards from the SFR–M_{dust} relation (having higher M_{dust} than what their SFRs would imply), as predicted for quenching that is not caused by the removal of gas (Hjorth et al. 2014; Leśniewska et al. 2023, M19). However, in simulations morphological quenching is found to be effective at gas fractions below a few percent (Martig et al. 2013; Gensior et al. 2020), much lower than for our sample (Figure 7).

The very low SFEs of our ETGs (Figure 6) indicate that star formation is suppressed even in comparison with other ETGs. This means that the process shutting down the SFRs in these galaxies is not due to physical gas removal, but to its inability to form stars. This again supports the internal quenching scenario, either morphological or connected with turbulence or magnetic fields.

For the ETGs in the ATLAS^{3D} sample, Kokusho et al. (2017) found no decline in SFE as a function of age, and found consistency with the SFR–M_{H_2} relation of star-forming galaxies. Hence, together with the decline in the gas fraction with age, this was interpreted as quenching driven by a decrease of the gas reservoir. In contrast, we do see a decline in the SFEs of our sample (Figure 6) and they are below the SFR–M_{H_2} relation (low SFRs for their molecular gas masses; Figure 5), again pointing at quenching being connected with the decreased ability of gas to form stars, not with a lack of gas.

Moreover, the high molecular gas fractions also point to a declining gas amount not being the main reason for the declining SFRs. Figure 7 shows the molecular gas fraction ($f_{H_2} \equiv M_{H_2}/M_*$) as a function of stellar mass compared with mass-selected low-redshift galaxies (Saintonge et al. 2017). The ETGs in our sample on the main sequence (lower ages) exhibit larger gas mass fractions than these star-forming galaxies, whereas the ETGs below the main sequence have comparable gas fractions to star-forming galaxies. Hence the lack of gas is not the main reason for the ETGs becoming passive. This is different from green-valley galaxies, for which both SFE and f_{H_2} were found to be suppressed (Brownson et al. 2020; Lin et al. 2022).

We note that our galaxies may not be representative of the entire ETG population, because they were selected based on Herschel 250 μm detections. This corresponds to a dust mass detection threshold of $10^{5.2}$ $M_\odot$ at $z = 0.05$ and $10^{6.7}$ $M_\odot$ at $z = 0.3$ (M19). These are not very high limits, especially given the high stellar masses of our galaxies, but most ETGs were shown to have less dust. In particular, in the ETG parent sample of Rowlands et al. (2012), only 5.5% were detected by Herschel. The remaining dust-poor ETGs may follow different evolutionary tracks than those presented here.

7. Mechanism(s) of ISM Removal

Here we discuss the possible physical mechanisms explaining the trend depicted in Figure 2. For each mechanism we list the predictions which can then be compared with existing and future data sets. The predictions are summarized in Table 5. Only two mechanisms are fully consistent with all the current data: removal of the entire cold ISM (Section 7.1) and outflows (Section 7.2). They are not mutually exclusive, so it could be that they operate together. In Section 8 we also discuss the energy source required for these mechanisms.

7.1. Removal of the Entire Cold Interstellar Medium

The destruction of all components of the cold ISM involves destroying the dust and molecular and atomic gas. We consider mechanisms having a stronger effect on dust in Section 7.3. There may be several physical mechanisms responsible for the removal of the entire ISM (planetary nebulae (PNe), Type Ia supernovae (SNe Ia), an AGN, hot gas, or cosmic rays). We will return to discussing these energy sources in Section 8.

The gas which is ceasing to be in the cold (molecular or atomic) phase is transformed into ionized hot gas. In our sample this requires heating a few times 10^9 $M_\odot$ of gas. The hot gas in elliptical galaxies has a mass corresponding to 1% of the

Table 5
Predictions of the Mechanisms That Can Explain the Dust Decline in Figure 2 and Their Consistency with the Currently Available Data

Mechanism	Prediction	Agreement with Data
Removal of the entire cold ISM (Section 7.1)	constant or decreasing $M_{\rm gas}/M_{\rm dust}$	✓, Figure 3
	M_* constant or slightly increasing with age	✓, Figure 1 in M19
	uniform or centrally concentrated ISM distribution	?
Outflows (Section 7.2)	constant or decreasing $M_{\rm gas}/M_{\rm dust}$	✓, Figure 3
	M_* constant or slightly increasing with age	✓, Figure 1 in M19
	off-center filamentary or plume-like gas structures	?
	multiple velocity peaks or broad line wings	?, Figure A1
Dust grain destruction (Section 7.3)	$M_{\rm gas}/M_{\rm dust}$ increasing with age	X, Figure 3
	M_* constant or slightly increasing with age	✓, Figure 1 in M19
Astration/strangulation (Section 7.4)	constant $M_{\rm gas}/M_{\rm dust}$	X, Figure 3
	M_* constant or slightly increasing with age	✓, Figure 1 in M19
	$M_{\rm dust}/M_*$ and $M_{\rm gas}/M_*$ flattening at higher ages	X, Figure 2
Decreasing number of AGB stars (Section 7.5)	AGB stars dominate dust production	X, 7.5
Dust cooling (Section 7.6)	submillimeter excess	X, Figure 5 in M19
	dust temperature decreasing with age	X, Figure 1 in M19
	$M_{\rm gas}/M_{\rm dust}$ increasing with age	X, Figure 3
Dust heating (Section 7.7)	SEDs peaking at short wavelengths	X, Figure A1 in R12
	dust temperature increasing with age	X, Figure 1 in M19
	$M_{\rm gas}/M_{\rm dust}$ increasing with age	X, Figure 3
Environmental influence (Section 7.8)	environmental density increasing with age	X, Figure 1 in M19
	rich environments	X, Figure 1 in M19
Mergers with gas-rich galaxies (Section 7.9)	$M_{\rm gas}/M_{\rm dust}$ increasing with the derived age	X, Figure 3
	M_* decreasing with the derived age	X, Figure 1 in M19
	$M_{\rm gas}/M_*$ decreasing with the derived age	✓, Figure 2
	$M_{\rm dust}$ only weakly correlated with M_*	X, Figure 3 in M19
	size increasing with decreasing age	X, Figure 2 in M19
M_*–age correlation (Section 7.10)	no $M_{\rm dust}/M_*$–age anticorrelation for narrow ranges of M_*	X, Figure A4
Selection bias (Section 7.11)	bias against old ISM-rich galaxies	X
	bias against young ISM-poor galaxies	X

Note. ✓: the prediction is consistent with the data, X: the prediction is inconsistent with the data, ?: the data needed to test this prediction are not available yet. R12: Rowlands et al. (2012).

stellar mass (or 10%–20% for the most massive ones; Mathews & Brighenti 2003; Sparke & Gallagher 2006). For our galaxies with stellar masses of $M_* = 10^{10-11}\ M_\odot$, this corresponds to $10^{8-9}\ M_\odot$ of hot gas (or more for the most massive galaxies in our sample). Hence, the amount of gas needed to be ionized by this mechanism is similar to the typical hot gas reservoirs in such galaxies, taking into account that some of the gas will be expelled or used for star formation.

This scenario predicts the following:

1. $M_{\rm gas}/M_{\rm dust}$ should be constant, as both dust and gas are destroyed, or decreasing with age if gas particles are destroyed faster due to their more diffuse distribution than dust, which has a more clumpy distribution.
2. M_* should be constant or slightly increase with age, given the low SFRs of the galaxies in our sample.
3. The gas and dust should be relatively uniformly distributed, possibly with either a central concentration, reflecting the initial distribution before the quenching, if the process removing the cold ISM is not violent and operates throughout galaxies, or a central deficit, if the source of the energy is in the galaxy center (AGN).

The $M_{\rm gas}/M_{\rm dust}$ ratio indeed declines slightly with age (Figure 3) and M_* is slightly increasing (Figure 1 in M19).

Our numerical model (Section 4, Figure A3, Table A1) shows that in order to explain the data, around 3–5 $\times\ 10^{10}\ M_\odot$ of gas (including both the atomic and molecular phase) needs to be removed on a timescale of 10 Gyr (for an average rate of 3–5 $M_\odot\ {\rm yr}^{-1}$, which includes the phase of being a normal star-forming galaxy). We note that this is much higher than the measured SFRs for higher ages, at which the gas decline is the strongest, so astration is unlikely to dominate the ISM mechanism (see Section 7.4).

7.2. *Outflows*

Gas and dust can be expelled from galaxies either by AGN- or stellar-induced winds. Outflows have been detected in M82 (Walter et al. 2002), Arp 220 (Perna et al. 2020), other starbursts (Tsai et al. 2009, 2012; Bolatto et al. 2013; Cicone et al. 2014;

Geach et al. 2014a, 2014b; Maiolino et al. 2017; Walter et al. 2017), and ETGs (Alatalo et al. 2011), and are present in simulations (Dalla Vecchia & Schaye 2012; Vogelsberger et al. 2014; Schaye et al. 2015; Davé et al. 2019; Burgarella et al. 2020; Nanni et al. 2020). Outflows can also be driven by cosmic rays (Hopkins et al. 2021a). This mechanism has been proposed as being responsible for shutting down star formation, at least in the most massive galaxies.

This scenario predicts the following:

1. $M_{\rm gas}/M_{\rm dust}$ should be constant with age, as both components are being removed, or decrease with age if the dust distribution is more clumpy (as in Section 7.1).
2. M_* should be constant or slightly increase with age, given the low SFRs of galaxies in our sample.
3. Some molecular gas should be located away from the optical centers of the galaxies, possibly in filamentary or plume-like structures with scales of around 1–2 kpc (Walter et al. 2002; Feruglio et al. 2010, 2015; Alatalo et al. 2011; Morganti et al. 2015).
4. Multiple velocity peaks with locations incompatible with a rotating disk, or broad line wings should be present (e.g., Cicone et al. 2014).

Predictions 1 and 2 are consistent with the data. We do not have spatial information on the distribution of gas to test prediction 3. In principle we can look for high-velocity wings in the spectra (Figure A1, prediction 4), but the expected signal is at the level of 10% of the main CO line peak (e.g., Cicone et al. 2014). Our data are not of enough signal-to-noise ratio to test this.

We also assessed how the required outflow rate compares with an empirical calibration. In our sample the molecular gas mass goes down from $\sim 10^{10}$ at an age of 1 Gyr to a few times 10^9 $M_\odot$ at 9 Gyr. Hence, the average outflow rate during this time must be around 1 $M_\odot$ yr^{-1}.

We estimated the actual outflow rate from the empirical calibration of Fluetsch et al. (2019; their Equation (5)) based on the SFR, M_*, and AGN luminosity ($L_{\rm AGN}$). We estimated the AGN luminosity from the [O III] luminosity ($L_{\rm [O\,III]}$), as done in Fluetsch et al. (2019) for cases with no X-ray data: $L_{\rm AGN} = 3500\ L_{\rm [O\,III]}$ (Heckman et al. 2004). Only five galaxies in our sample have $>3\sigma$ detection of the [O III] line, so we first calculated the molecular outflow rates setting the AGN luminosity to zero. These are shown as circles in Figure 8. Then we calculated the maximum outflow rate by setting the AGN luminosity to the 2σ upper limit allowed by the [O III] data (arrows on this figure). It is clear that the measured outflow rates are at the level of the required average rate only at the beginning of the evolution. Hence, the outflows calculated in this way are not powerful enough to explain the gas mass decline throughout the entire period.

To demonstrate this we fitted an exponential function to the outflow rate as a function of age and obtained the functional form of the outflow rate in units of $M_\odot$ yr^{-1} of $(3.9 \pm 1.0)\exp\{-{\rm age}/[(1.36 \pm 0.24)\ {\rm Gyr}]\}3[$ (the half-life time is 0.41 ± 0.07 Gyr, shown with a dashed line on Figure 8). Then, starting with a molecular mass of 10^{10} $M_\odot$ at an age of 1 Gyr we show in Figure A2 in the Appendix how much gas and dust is removed with an outflow of such strength. It is clear that the evolution is nearly flat, as the outflow rate is too low (especially at older ages) to explain the gas decline.

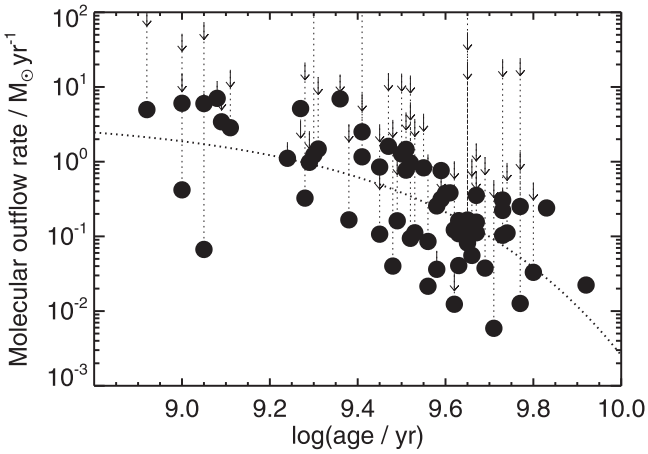

Figure 8. Molecular outflow rate (Equation (5) of Fluetsch et al. 2019) as a function of the luminosity-weighted stellar age. Circles denote measurements made without taking into account the AGN contribution (because most of the galaxies in our sample have not been detected at [O III]). Arrows denote the molecular outflow rates with the maximum (2σ) contribution from an AGN allowed by the [O III] data. The dashed line is an exponential fit to the data with the form (outflow rate/$M_\odot$ yr^{-1}) $= (3.9 \pm 1.0)\exp\{-{\rm age}/[(1.36 \pm 0.24)\ {\rm Gyr}]\}6$. These outflow rates are too low to explain the ISM decline (see Figure A2).

7.3. Dust Grain Destruction

Dust grains can be destroyed by, e.g., SN shocks, an AGN, or by sputtering in the hot gas. This scenario predicts the following:

1. $M_{\rm gas}/M_{\rm dust}$ should increase with age as gas is not destroyed, just dust.
2. M_* should be constant or slightly increase with age, given the low SFRs of galaxies in our sample.

This mechanism is ruled out by prediction 1. The gas-to-dust ratio does not increase with age (Figure 3), as directly predicted by this mechanism. The gas masses are also decreasing with time (Figure 2).

7.4. Astration/Strangulation

Gas and dust are incorporated into newly formed stars (astration), so if the SFR is higher than the gas inflow rate, or if the gas inflow is stopped (a process called strangulation; Peng et al. 2015; Trussler et al. 2020), then the gas reservoir will be depleted This scenario predicts the following:

1. $M_{\rm gas}/M_{\rm dust}$ should be constant with age, as both components are being removed, or slightly increase if the dust distribution is more clumpy as this is where star formation is occurring.
2. M_* should be constant or slightly increase with age, given the low SFRs of galaxies in our sample.
3. Given the decreasing SFR with age (Figure 1 in M19), the dust and gas removal should be weaker for older ages, so the drop of $M_{\rm dust}/M_*$ and $M_{\rm gas}/M_*$ should flatten at older ages (see the $M_{\rm dust}$ panel in Figure 1 in M19).

This mechanism is ruled out by prediction 3 and, with a lower statistical significance, by prediction 1. First, Figure 2 clearly shows steepening of the decline of the $M_{\rm dust}/M_*$ ratio, so the dust removal is stronger for higher ages. Hence this cannot be connected with the SFR, which is the lowest at high ages. Indeed, M19 showed that the effect of astration with

measured SFRs on the dust amount is minor, and is unable to explain the dust decline.

In order to quantify what effect the astration might have on gas evolution we made calculations similar to those presented in M19 for dust evolution. Figure 1 in M19 presents an exponential fit to the SFR evolution (see Equation (8) above). We used this, starting with 10^{10} $M_{\odot}$ of gas to see the effect of astration. This is shown in Figure A2 in the Appendix. The evolution is nearly flat, showing that the SFRs are not high enough, so astration cannot be responsible for most of the gas and dust decline. Hence, we conclude that, while astration is happening, the effect is too weak to explain the data fully. This is consistent with the conclusion drawn in M19.

Similarly, Figure A3 in the Appendix shows that models with only astration are inconsistent with the data because the gas removal is the weakest for high ages. Only incorporating additional gas removal makes the models agree with the data.

Finally, the gas-to-dust ratio is not constant (or increasing) with age (Figure 3). The Spearman's correlation coefficient for that plot is -0.85 with the probability of a null hypothesis (no decline) being $\sim$0.0037 ($\sim 3\sigma$).

7.5. A Decline in the Number of Dust-producing AGB Stars

It could be that the decline of $M_{\rm dust}/M_{*}$ and $M_{\rm gas}/M_{*}$ is due to a decline in the number of dust-producing AGB stars at older ages, which also release gas to the ISM. This is only possible if the dust and gas produced by these AGB stars dominate the current dust and gas budget in these galaxies. Otherwise, if their contributions are minor, then the decline in their numbers cannot explain the decline in the dust or gas content.

Rowlands et al. (2012) and M19 showed that indeed AGB stars do not contribute significantly to the dust production in these galaxies. Given their stellar masses, the number of AGB stars is too low and each of these stars would need to have produced a too high amount of dust.

We now examine whether the gas masses we detected in the ETGs could have had a large contribution from the ejecta of AGB stars. We compare the gas masses with the expected numbers of AGB stars calculated from the stellar masses, using a similar argument as presented in Michałowski et al. (2010a, 2010b), Michałowski (2015), and Leśniewska & Michałowski (2019; see also Morgan & Edmunds 2003; Dwek et al. 2007; Dwek & Cherchneff 2011; Rowlands et al. 2014). A stellar mass of 10^{11} $M_{\odot}$ implies around 10^{10} AGB stars (1.5–8 $M_{\odot}$), assuming the Chabrier (2003) IMF. A gas mass of $\sim 10^{10}$ $M_{\odot}$ for the galaxies in our sample at the lowest ages implies that each AGB star would need to release approximately 1 $M_{\odot}$ of gas. This is, to an order of magnitude, the total ejecta mass expected per AGB star (Morgan & Edmunds 2003; Ferrarotti & Gail 2006). This calculation neglects past gas consumption due to star formation and outflows (which would increase the required total ejecta mass per star) and inflows (which would decrease the required ejecta mass). It seems that AGB stars are numerous enough to explain the observed gas masses. However, as mentioned above, they do not contribute significantly to dust production, so it is likely that the gas decline is connected with the same mechanism as the dust decline, and not a decreasing number of AGB stars. On the other hand, this calculation supports the internal origin of the ISM in these ETGs, as claimed in M19.

This leaves the question why the majority of ETGs selected in a similar way to our sample do not have detectable ISM contents, given that they have similar stellar masses, and so a similar number of AGB stars. We speculate that this may be due to the nondetected galaxies being older, or exhibiting a stronger ISM destruction mechanism (e.g., a more powerful AGN), or having a higher amount of very hot gas, leading to immediate ionization of all of the gas released by the AGB stars.

7.6. Dust Cooling

It could be that with time the dust is not destroyed, but cools down, so that it becomes invisible for Herschel. This scenario predicts the following:

1. As a result of this extra cold dust component, longer-wavelength observations should result in high flux levels above the extrapolation from the Herschel wavelengths.
2. The dust temperatures measured with the Herschel data should decrease with age.
3. The gas-to-dust ratios should increase, because the gas mass measurement is unaffected.

The data are inconsistent with all these predictions. Our James Clerk Maxwell Telescope/SCUBA-2 data rule out this mechanism, because we do not see a flux excess at 850 μm (Figure 5 in M19). Moreover, we do not see any trend of the dust temperature with age, and the range of the temperatures is relatively narrow (Figure 1 in M19). Finally, the gas content also decreases (Figure 2) and hence, the gas-to-dust ratios are constant or slightly decrease (Figure 3).

7.7. Dust Heating

If dust is progressively heated to high temperatures (but not destroyed), then it could become invisible for Herschel/SPIRE. This scenario predicts the following:

1. The SEDs of these galaxies should have their peak shifted toward shorter wavelengths.
2. The dust temperature measured with the Herschel data should increase with age.
3. The gas-to-dust ratios should increase, because the gas mass measurement is unaffected.

The data are inconsistent with all these predictions. The SEDs of the galaxies in our sample do not show any evidence of a shift of the peak toward shorter wavelengths (Rowlands et al. 2012). Moreover, we do not see any trend of the dust temperature with age (Figure 1 in M19). Finally, the gas-to-dust ratios do not increase with age (Figure 3).

An additional warm component with a temperature of 30 K could only contribute a few percent to the cold dust mass in order not to overshoot the 100 μm detections or limits. The contribution of even hotter dust could be even lower because even a small amount of hot dust is too bright. Hence, the possible contribution of hot dust is too small to explain the decrease of the $M_{\rm dust}/M_{*}$ ratio.

7.8. Environmental Influence

In principle it is possible that the observed trend is the reflection of environmental influence. Galaxies in richer environments are quenched quicker (so the stellar ages are higher) and the ISM is being removed quicker due to environmental effects like interactions or ram pressure stripping.

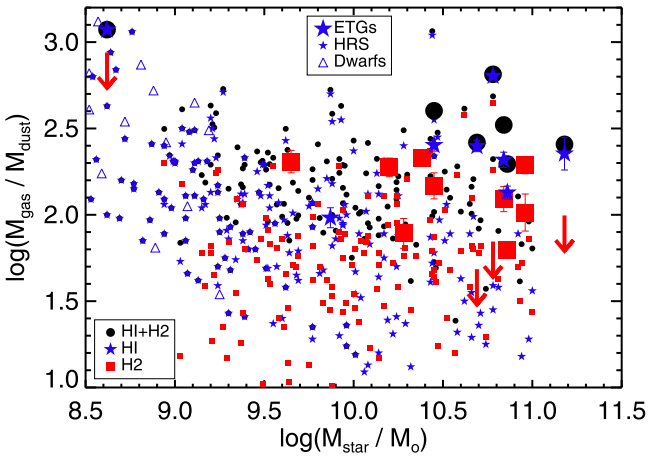

Figure 9. Gas-to-dust ratios as a function of stellar mass. Large symbols denote the galaxies in our ETG sample, and small symbols denote those from HRS. Red squares, blue stars, and black circles denote molecular gas, atomic gas, and total gas, respectively (the latter only for galaxies with both CO and H I measurements). The ETGs in our sample have high gas-to-dust ratios, but are consistent with the HRS population, arguing against an external source of their ISMs via mergers with dwarf galaxies, which have high gas-to-dust ratios.

This scenario predicts the following:

1. There should be a trend of environment density with age (and therefore with the $M_{\rm dust}/M_*$ ratio).
2. These galaxies should live in rich environments in which the influence on their ISM is significant.

None of these predictions are consistent with the data. As shown in Figure 1 in M19, the galaxy density does not depend on age. Moreover, these galaxies do not reside in rich environments. The projected galaxy densities are below 10 Mpc^{-2}, below that of galaxy groups. We also do not see any dependence of the dust decline on environment in the extended analysis of 2000 dusty ETGs (Leśniewska et al. 2023).

7.9. Mergers with Gas-rich Galaxies

It could be that the trend cannot be interpreted as a time evolution, but results from mergers of passive gas-poor galaxies with gas-rich star-forming galaxies of different masses, or that each passive galaxy experienced different number of mergers. If the merging star-forming galaxy was relatively large (or a passive galaxy had experienced more mergers), then the resulting mean age would be low (because of the many young stars brought in during the mergers) and the resulting $M_{\rm dust}/M_*$ would be high (because more dust is brought in). A merger with a small star-forming galaxy (or fewer number of mergers) would result in a much higher derived age and a much lower $M_{\rm dust}/M_*$ ratio. This scenario predicts the following:

1. $M_{\rm gas}/M_{\rm dust}$ should be increasing with the derived age, because passive galaxies with high derived ages would need to have merged with smaller galaxies, which have high $M_{\rm gas}/M_{\rm dust}$ ratios (Grossi et al. 2010, 2015; Galametz et al. 2011; Leroy et al. 2011; Cortese et al. 2012b; Hunt et al. 2014; Rémy-Ruyer et al. 2014).
2. M_* should be constant or slightly decrease with the derived age because merging dwarf galaxies would not contribute much to M_*, and the galaxies in our sample with lower inferred ages would have on average experienced more merging and so may be slightly more massive.
3. $M_{\rm gas}/M_*$ should be decreasing with the derived age, for the same reason why $M_{\rm dust}/M_*$ is decreasing (higher-mass galaxies bring more gas).
4. $M_{\rm dust}$ should only be weakly correlated with M_*, because the gas-rich companions would not bring significant amounts of stars, so the final M_* should only weakly depend on the number of merger events.
5. The sizes should be increasing with decreasing age, because in this scenario a low derived age means more merging and the galaxies grow in size as a result of mergers (Naab et al. 2009; Hopkins et al. 2010; Trujillo et al. 2011; Furlong et al. 2017).

This mechanism is ruled out by predictions 1, 2, 4, and 5. It has also been ruled out by Rowlands et al. (2012) and M19 in the context of the analysis of the source of dust in these galaxies (see also Donevski et al. 2023).

The gas-to-dust ratio is not increasing with age (Figure 3), inconsistent with prediction 1. Figure 1 in M19 shows that the stellar mass is increasing slightly with age, which should not be the case if the apparent dust decline with age was a result of merging with smaller (or fewer) galaxies at high ages and larger (or more numerous) galaxies at low ages (prediction 2). Moreover, Figure 3 in M19 shows that $M_{\rm dust}$ is correlated with M_*, inconsistent with prediction 4. The Spearman's rank correlation coefficient is 0.5 with a very small probability ($\sim 3 \times 10^{-5}$, $\sim 4\sigma$) of the null hypothesis (no correlation) being acceptable. Figure 2 in M19 also shows that there is no correlation of the sizes of these galaxies with age, as would be expected if mergers are the mechanism responsible for the trends we observe (prediction 5).

Conversely, Davis et al. (2015) concluded that the gas in most ETGs with dust lanes has an external origin, because of the large range of gas-to-dust ratios extending to high values ($\sim$800), typical for dwarf galaxies, which have apparently merged with gas-poor ETGs (see also Lianou et al. 2016). For our sample the gas-to-dust ratios are smaller, suggesting high-metallicity ISMs, and hence an internal origin. We show the gas-to-dust ratios as a function of stellar mass in Figure 9. We compare our galaxies with spirals from the Herschel Reference Survey (HRS; Boselli et al. 2010, 2014; Bendo et al. 2012; Ciesla et al. 2012, 2014; Cortese et al. 2012a, 2014). Their dust likely has an internal origin (because they are currently forming stars) and the ETGs in our sample fully overlap with these spirals, which supports the internal origin of dust in these ETGs. On the other hand, dwarf galaxies exhibit much higher atomic gas-to-dust ratios of 300–10,000 (Grossi et al. 2010, 2016; Cormier et al. 2014; Hunt et al. 2014, 2015, 2017).

7.10. Stellar Mass–Age Correlation

More massive galaxies are on average older (e.g., McDermid et al. 2015), so in principle the $M_{\rm dust}/M_*$–age anticorrelation could be driven by the M_*–age correlation. This scenario predicts that this anticorrelation should disappear if only a narrow range of stellar masses is analyzed.

The sample analyzed in this paper is too small to subdivide it in narrow bins of stellar mass, but this can be done for galaxies selected similarly by Leśniewska et al. (2023) in a much bigger field. Figure A4 in the Appendix shows that the $M_{\rm dust}/M_*$–age anticorrelation persists even for very narrow ranges of stellar

masses, which is inconsistent with it being driven by the M_*–age correlation. The scatter in the stellar mass bins $\log(M_*/M_\odot) =$ 10.5–10.6 and 10.6–10.7 is 0.39 and 0.36 dex, respectively, which show that it does not increase compared to the full sample with a scatter of 0.43 dex.

7.11. Selection Bias

Our sample has been selected based on redshift, elliptical morphology, and dust detection, and is a 250 μm flux-limited sample. If the $M_{\rm dust}/M_*$–age decline was the a result of a selection bias, then this would need to imply that:

1. The selection criteria should remove old, very dust-rich galaxies.
2. The selection criteria should remove young galaxies with dust contents similar to those detected in older galaxies.

None of these biases are introduced by our selection criteria. If old galaxies with high dust content or young galaxies with dust content equally low as we see for older galaxies existed, we would have detected them.

8. Energy Source

While the observations favor a scenario involving the removal of the entire cold ISM or outflows, the question remains what is the source of energy responsible for the ISM removal? This cannot be connected with the current star formation, because the SFRs are low in the galaxies in our sample and the SFR level gets progressively lower, which would result in a flattening evolution of the ISM content, inconsistent with the observations. We consider PNe, SNe Ia, cosmic rays, hot halo gas, and AGNs. PNe or SNe Ia (either directly or through cosmic rays) or AGNs (if their duty cycle is low) are the most likely explanations. They are short lived sources of energy, so consecutive generations of stars need to go through these phases constantly to make these scenarios possible.

For all potential energy sources, we will discuss how the state of the cold gas changes. It can either be removed from the galaxy entirely or transformed into warm ionized gas (temperature of 10^{4-5} K) or hot ionized gas (temperature $>10^6$ K). Given the lack of X-ray data, we do not have a constrain on the latter, but we calculated the amount of warm ionized gas from the Hα luminosity using Equation (1) of Pagotto et al. (2021), following their assumption of electron density $n_e = 100$ cm^{-3}. The resulting masses of warm ionized gas of 10^{4-5} $M_\odot$ are much lower than the difference between the cold gas masses of the youngest and oldest galaxies analyzed here of 10^9 $M_\odot$. Hence, cold gas cannot be transformed into the warm ionized phase for these galaxies and can only be heated to much higher temperatures or removed by outflows.

8.1. Planetary Nebulae

Low-mass stars during the main-sequence or AGB phases are not energetic enough to ionize the gas around them (which is required to explain the decline of both molecular and atomic gas). However, the post-AGB/PN phase is a possibility, usually referred to as a hot low-mass evolved star (Binette et al. 1994; Flores-Fajardo et al. 2011; Herpich et al. 2018). During this phase a star ejects its envelope with an expansion velocity of around 30 km s^{-1}, and this gas has temperature $\sim 10^{4-5}$ K (e.g., Cuisinier et al. 1996; Milingo et al. 2002; Sharpee et al. 2007; Sahai & Chronopoulos 2010; Bohigas et al. 2015; Ali et al. 2015; Ali & Dopita 2019). This is enough to move gas to the warm ionized phase, but is not enough to expel gas from a galaxy or to heat it to very high temperatures of $>10^6$ K. However, in environments with a high stellar velocity dispersion, the interaction of PNe with the ambient gas can lead to heating to such high temperatures (Conroy et al. 2015). This scenario was invoked by Conroy et al. (2015) as a mechanism responsible for preventing star formation in quiescent galaxies. There are indeed indications that post-AGB stars are responsible for the photoionization of gas in ETGs (Binette et al. 1994; Stasińska et al. 2008; Cid Fernandes et al. 2010, 2011; Sarzi et al. 2010; Kehrig et al. 2012; Yan & Blanton 2012; Papaderos et al. 2013; Singh et al. 2013; Gomes et al. 2016; Herpich et al. 2018).

We made simple calculations to estimate whether PNe are numerous enough in the galaxies in our sample to explain the gas decline. A galaxy with a total stellar mass of $\sim 10^{11}$ $M_\odot$ has $\sim 1.9 \times 10^{10}$ stars with masses between 1 and 8 $M_\odot$, which ended their lives as PNe. In our sample the total gas mass goes down from $\sim 10^{10}$ $M_\odot$ at an age of 1 Gyr to $\sim 2 \times 10^9$ $M_\odot$ at 9 Gyr. Hence, one PN would need to remove $\sim 8 \times 10^9$ $M_\odot$/ $1.9 \times 10^{10} = 0.4$ $M_\odot$ of gas.

This calculations does not take into account that some stars go through the PN phase before the period considered here for gas removal of 8 Gyr. At $z = 0.1$–0.3 there are an additional 2–4 Gyr after the Big Bang. If we make the most conservative assumption that all stars were created at the time of the Big Bang, then during this extra time stars with masses of more than 1.4–1.9 $M_\odot$ have already went through the PN phase before our considered ISM-removal phase. This decreases the number of available PNe to 1.1–0.8×10^{10} and therefore increases the required gas removal to 0.7–1 $M_\odot$ per PN.

The largest (i.e., oldest) PNe or circumstellar envelopes of evolved stars have radii of the order of 1 pc (e.g., O'Dell et al. 2004; Sahai & Chronopoulos 2010; Matthews et al. 2015). For an ISM density of 20–50 cm^{-3} for the cold atomic medium (Ferrière 2001), this corresponds to $\sim$2–5 $M_\odot$ of swept-up gas. This is similar to our estimate of the required gas removal per PN, so they are numerous enough to be responsible for the detected gas decline.

8.2. Type Ia Supernovae

SNe Ia can ionize gas and destroy dust in the swept up part of the ISM (Li et al. 2020). The swept-up gas can reach temperatures of $>10^6$ K (Ceverino & Klypin 2009; Hopkins et al. 2018a; Li et al. 2020), required to move it to the very hot gas phase.

Similarly as for the PNe we estimate the required effectiveness of SNe Ia. Using Equation (19) and Table 1 of Andersen & Hjorth (2018) we estimate the rate of SNe Ia for a galaxy with $M_* = 10^{11}$ $M_\odot$ and SFR = 0–10 $M_\odot$ yr^{-1} to be 0.008–0.014 yr^{-1}. For a period of 8 Gyr this corresponds to ~ 1.1–6.4×10^7 SNe Ia. Hence, one SN Ia would need to remove $\sim$730–130 $M_\odot$ of gas.

SNe Ia release around 10^{51} erg of energy (Khokhlov et al. 1993). For a SN with such energy in the simulations of Yepes et al. (1997) $\sim$20–5000 $M_\odot$ of gas is ionized. The required strength of SN feedback for our sample is consistent with this range. We therefore find this mechanism feasible.

We do not consider CCSNe here because the lifetimes of their progenitors are very short, so their numbers are closely

connected with recent star formation. Therefore their numbers decrease for galaxies with high ages, which makes them unable to explain the detected gas decline, similar to astration.

8.3. Cosmic Rays

Interactions with cosmic rays can lead to the destruction of dust particles by thermal evaporation and sputtering (Dwek & Arendt 1992), and also to the heating and ionization of gas (Hayakawa et al. 1961; Spitzer & Tomasko 1968; Ferrière 2001; Indriolo et al. 2009; Padovani et al. 2020; Gabici 2022). The lifetime of a cosmic ray is only 10^{6-7} yr (Jokipii & Parker 1969; Garcia-Munoz et al. 1975, 1977; Jokipii 1976; Yanasak et al. 2001; Bisbas et al. 2015, 2017; Gabici 2022). Hence, cosmic rays produced by CCSNe are unlikely to affect the ISMs of the galaxies in our sample, due to their low SFRs, resulting in a low number of currently exploding CCSNe unable to ionize the amount of gas we detect. However, cosmic rays can also be produced by SNe Ia (Chan et al. 2019).

Simulations show that cosmic rays are capable of dispersing or launching gas clouds on timescales of the order of 10 Myr (Brüggen & Scannapieco 2020). This is much shorter than the timescale over which the gas content declines in our sample. Therefore, in order for this mechanism to be viable, large amounts of cold dust would need to be shielded in dense clouds against the influence of cosmic rays, which would make the timescale much longer and consistent with our measurements.

It has been shown with simulations that cosmic rays can reduce the SFRs of galaxies by a factor of 5 and the density of gas in galaxy centers by an order of magnitude (Hopkins et al. 2021b; Byrne et al. 2023). However, they do not heat gas to temperatures beyond 10^6 K, as required here. Hence, the only viable mechanism to explain the decline in cold gas reservoir detected in our sample is a cosmic-ray–driven outflow.

Summarizing, cosmic rays produced by SNe Ia can also be responsible for the ISM decline we detect if they drive outflows.

8.4. Active Galactic Nuclei

AGN feedback has been invoked as a mechanism of quenching for massive galaxies as they can heat gas to very high temperatures (see the review of Fabian 2012).

As stated in Section 7.2, only five galaxies in our sample have a $>3\sigma$ detection of the [O III] line, which is used as an AGN indicator. The median 2σ upper limit on the AGN luminosity, calculated as $L_{\rm AGN} = 3500\ L_{\rm [O\ III]}$ (Heckman et al. 2004) is 2×10^{42} erg s^{-1}. This indicates a low level of current AGN activity. This is consistent with our analysis of emission lines of 2000 dusty ETGs, where we found that only up to 15% exhibit line ratios typical for AGNs (O. Ryzhov et al. 2024, in preparation).

However, the timescale during which a typical AGN is active is much shorter than the gigayear timescale considered here (Novak et al. 2011; Hickox et al. 2014; Padovani et al. 2017). Therefore, the visibility of AGNs in a given population depends mainly on the duty cycle (fraction of time during which the AGN is active). For a conservatively low Eddington ratio of 0.01, simulations predict a duty cycle of ∼1%–10% (Novak et al. 2011, their Figure 8), so in a sample fully dominated by AGNs, only this fraction is expected to show current AGN activity. For a higher Eddington ratios (stronger AGN activity) the expected detected fraction is even lower. These fractions are similar to what we obtain, meaning AGN feedback can be a possible mechanism of removing the ISMs in these galaxies.

8.5. Hot Halo Gas

Hot, X-ray-emitting gas is frequently found in elliptical galaxies with stellar masses similar to those in our sample (e.g., Sarzi et al. 2013; Su et al. 2015; Kim et al. 2019; Kokusho et al. 2019). The dust destruction timescales in hot (10,000 K or more) media are estimated to be 10^4–10^8 yr (Draine & Salpeter 1979; Jones et al. 1994; Jones 2004; Micelotta et al. 2010; Bocchio et al. 2012; Hirashita et al. 2015; Hirashita & Nozawa 2017). This is much shorter than the dust and gas removal timescale measured here, in M19, and in Leśniewska et al. (2023). However, if the cold ISM is partially shielded from the influence of hot gas, then the destruction process would be slower and could be responsible for the decline we detect.

Smercina et al. (2018) interpreted the dust decline in poststarburst galaxies as the effect of grain sputtering in a hot medium. However, they did not detect a gas decline, in contrast to the galaxies in our sample. Galliano et al. (2021) interpreted the low dust-to-gas ratios of ETGs as the result of dust grain sputtering in hot gas, but our sample exhibits much higher dust-to-gas ratios (compare Figure 3 with their Figure 8).

Finally, dust destruction in hot halo gas applies only to low-density media (Bocchio et al. 2012). Hence, it is unlikely to be the main mechanism in the galaxies in our sample, given their substantial ISM masses.

9. Conclusions

We present CO and 21 cm hydrogen (H I) line observations of dusty ETGs and measure the removal of their cold ISMs. We find that all the cold ISM components (dust and molecular and atomic gas) decline at similar rates. This allows us to rule out a wide range of potential ISM-removal mechanisms (including starburst-driven outflows, astration, or a decline in the number of AGB stars), and artificial effects like the stellar mass–age correlation, environmental influence, mergers, and selection bias, leaving ionization by evolved low-mass stars or ionization/outflows by SNe Ia or AGNs as viable mechanisms. We also provide the support of an internal origin of the detected ISMs. Moreover, we find that the quenching of star formation in these galaxies cannot be explained by a reduction in gas amount alone, because the SFRs decrease faster (at a timescale of about 1.8 Gyr) than the amount of cold gas (a timescale of 2.3 Gyr). Furthermore, the SFEs of the ETGs (SFE $\equiv$ SFR/$M_{\rm H_2}$) are lower than those of star-forming galaxies, whereas their gas mass fractions ($f_{\rm H_2} \equiv M_{\rm H_2}/M_*$) are normal. This may be explained by the stabilization of gas against fragmentation, for example due to morphological quenching, turbulence, or magnetic fields.

Acknowledgments

We thank Joanna Baradziej for help with improving this paper, Claudia Marka for excellent support with the IRAM 30 m observations and reduction, and the IRAM 30 m staff and observers for executing our programs.

M.J.M., A.L., J.N., O.R., and M.S. acknowledge the support of the National Science Centre, Poland through the SONATA BIS grant 2018/30/E/ST9/00208. M.J.M. acknowledges the support

of the Polish National Agency for Academic Exchange Bekker grant BPN/BEK/2022/1/00110, the National Science Centre, Poland through the POLONEZ grant 2015/19/P/ST9/04010, the Polish-U.S. Fulbright Commission, UK Science and Technology Facilities Council, British Council Researcher Links Travel Grant, Royal Society of Edinburgh International Exchange Programme, and the hospitality of the Instituto Nacional de Astrofísica, Óptica y Electrónica (INAOE), the Academia Sinica Institute of Astronomy and Astrophysics (ASIAA), University of Edinburgh, and the Dark Cosmology Centre. This project has received funding from the European Union's Horizon 2020 research and innovation program under the Marie Skłodowska-Curie grant agreement No. 665778. C.G. acknowledges funding from the Carlsberg Foundation and the Carnegie Trust Research Incentive Grant (PI: M. Michałowski) as well as support through a VILLUM FONDEN Young Investigator Grant (project number 25501). J.H. was supported by a VILLUM FONDEN Investigator grant (project number 16599). A.-L.T. acknowledges the support of the National Science Centre, Poland through the POLONEZ grant 2015/19/P/ST9/04010. T.T.T. has been supported by the Grant-in-Aid for Scientific Research (Nos. 17H01110 and 21H01128). P.B. acknowledges funding through the Spanish Government retraining plan "María Zambrano 2021-2023" at the University of Alicante (ZAMBRANO22-04) This research was funded in whole or in part by the National Science Centre, Poland (grant Nos. 2021/41/N/ST9/02662 and 2020/39/D/ST9/03078). For the purpose of Open Access, the author has applied a CC-BY public copyright licence to any Author Accepted Manuscript (AAM) version arising from this submission. This article has been supported by the Polish National Agency for Academic Exchange under grant No. PPI/APM/2018/1/00036/U/001. O.R. acknowledges the support of the National Science Centre, Poland through the grant 2022/01/4/ST9/00037.

This work is based on observations carried out under project numbers 198-14, 62-15, and 174-15 with the IRAM 30 m telescope. IRAM is supported by INSU/CNRS (France), MPG (Germany), and IGN (Spain). The research leading to these results has received funding from the European Commission Seventh Framework Programme (FP/2007-2013) under grant agreement No. 283393 (RadioNet3). The Green Bank Observatory is a facility of the National Science Foundation operated under cooperative agreement by Associated Universities, Inc. This research used the facilities of the Canadian Astronomy Data Centre operated by the National Research Council of Canada with the support of the Canadian Space Agency.

This research has made use of the Tool for OPerations on Catalogues And Tables (TOPCAT; Taylor 2005) at www.starlink.ac.uk/topcat/, SAOImage DS9, developed by Smithsonian Astrophysical Observatory (Joye & Mandel 2003), NASA's Astrophysics Data System Bibliographic Services, and the WebPlotDigitizer[22] of Ankit Rohatgi.

Appendix
Additional Figures and Tables

We present here additional figures showing the CO and H I spectra (Figure A1), effect of outflows and astration (Figures A2 and A3), the effect of the mass–age correlation (Figure A4), as well as a table with model parameters (Table A1).

[22] https://automeris.io/WebPlotDigitizer

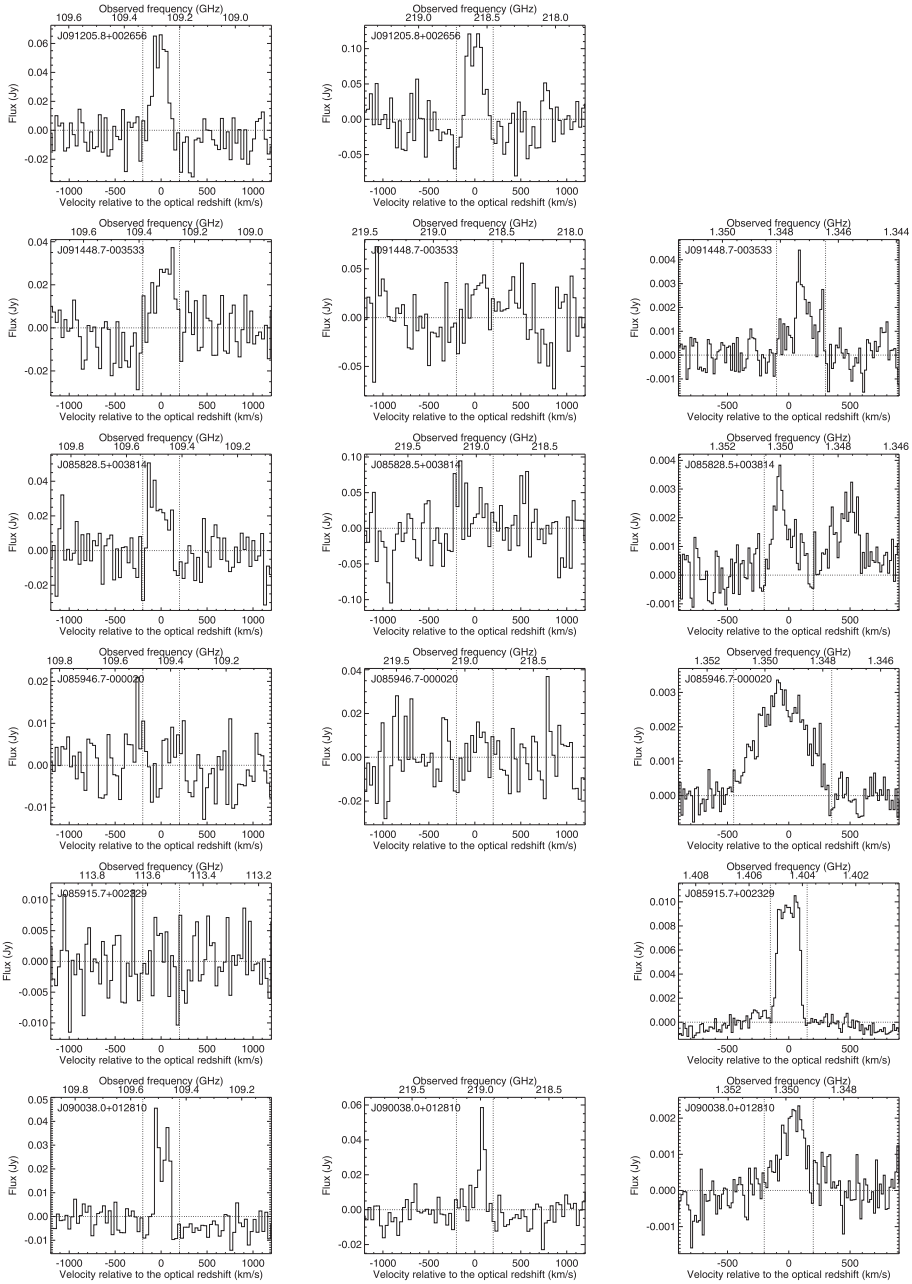

Figure A1. CO(1–0) (left), CO(2–1) (middle), and H I (right) spectra from the IRAM 30 m and GBT observations. The vertical dotted lines show the velocity range over which the spectra were integrated in order to obtain the line fluxes.

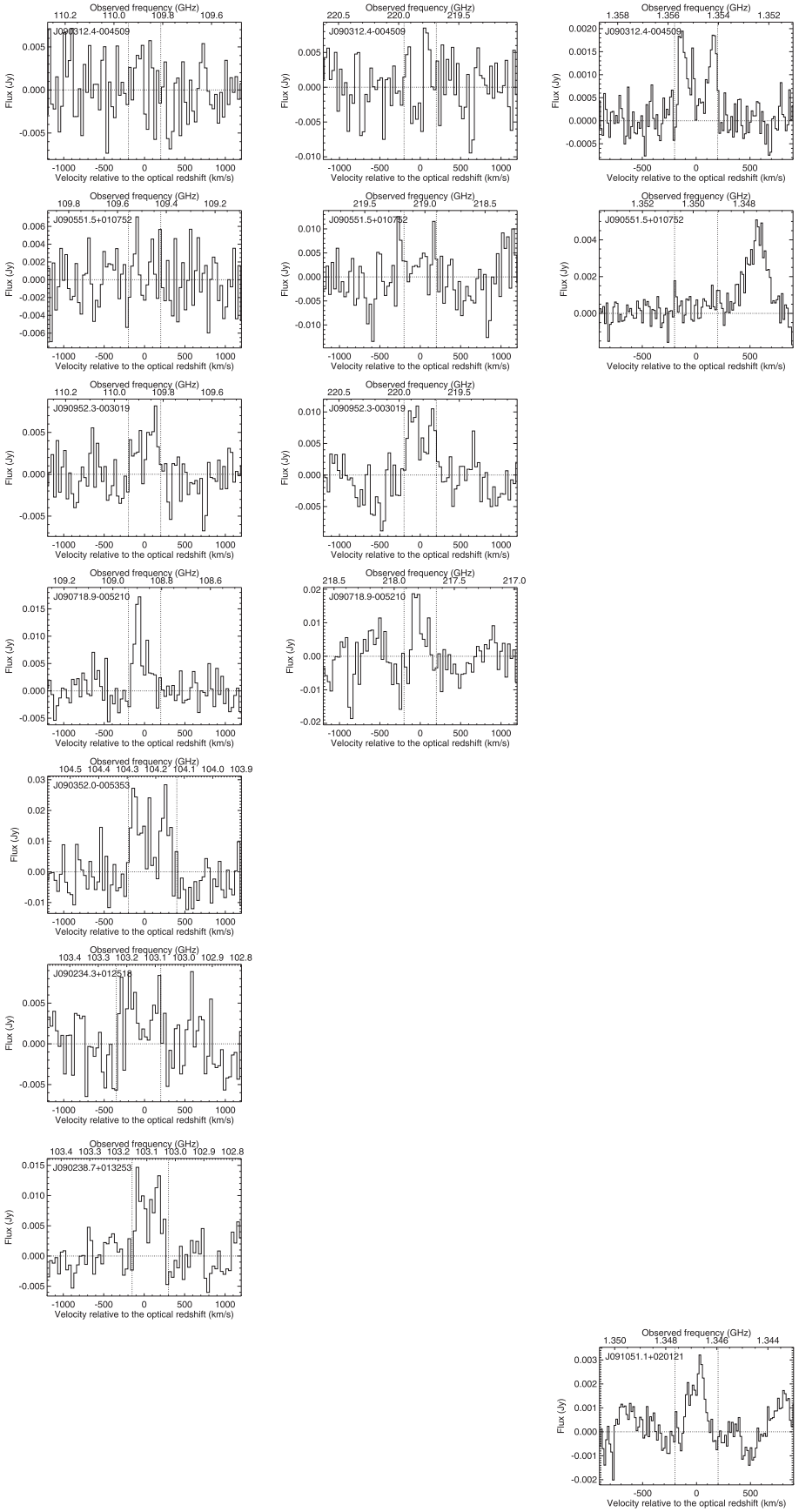

Figure A1. (Continued.)

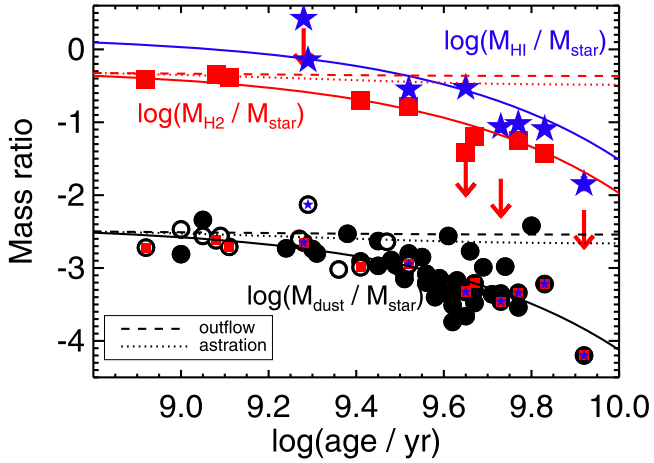

Figure A2. The same as Figure 2, but showing the effect of outflows and astration. The dotted and dashed lines denote the molecular gas and dust mass evolution assuming that outflows (with a rate as measured in Figure 8) and astration (with the SFR as measured in Figure 1 of M19) are the only cause of the gas mass change, respectively. This shows that these two effects are too weak to explain the data.

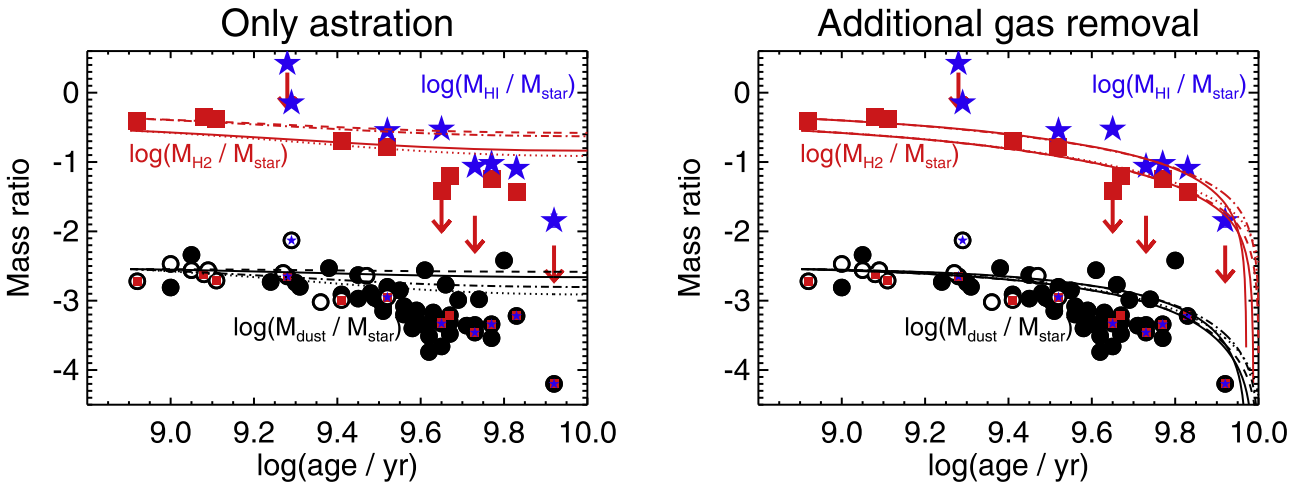

Figure A3. The same as Figure 2, but showing the results of the models of GAH11 presented in Section 4. The left panel show the models with astration (with the SFR as measured in Figure 1 of M19) as the only mechanism of ISM removal. In the right panel models with additional cold gas removal (gas heating or outflows) are shown. The model parameters are shown in Table A1. This shows that some additional gas removal mechanism is necessary to explain the data.

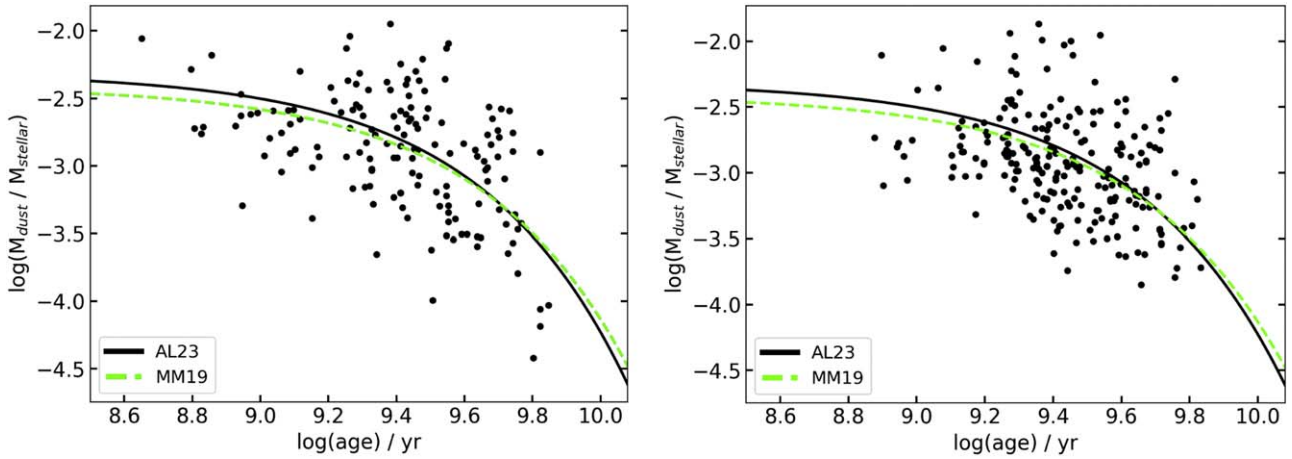

Figure A4. The same as Figure 2, but for the larger sample of Leśniewska et al. (2023) only for a narrow range of stellar masses: $\log(M_*/M_\odot) = 10.5$–10.6 (left) and 10.6–10.7 (right). The solid black line shows the fit to the full sample of Leśniewska et al. (2023) and the dashed green line shows the fit to the sample in M19. This shows that the $M_{\rm dust}/M_*$–age anticorrelation is not driven by the M_*–age correlation, because it would disappear for narrow ranges of M_*.

Table A1
Chemical Evolution Model Main Parameters

M_{ISM} (10^{10} $M_\odot$)	SN[a] Recycling	AGB[a] Recycling	M_{out} (10^{10} $M_\odot$)	t_{out} (10^{10} yr)
Only astration				
2.0	√	no	⋯	⋯
2.0	no	no	⋯	⋯
3.0	√	no	⋯	⋯
3.0	no	no	⋯	⋯
With additional gas removal				
2.0	√	√	2.9	1.0
2.0	√	√	2.8	1.0
2.0	√	√	2.7	0.9
3.0	√	√	4.4	0.9
3.0	√	√	5.4	1.2

Note.
[a] Refers to whether the mass recycled from dying stars is considered to be instantaneously available for star formation or not.

ORCID iDs

Michał J. Michałowski https://orcid.org/0000-0001-9033-4140
C. Gall https://orcid.org/0000-0002-8526-3963
J. Hjorth https://orcid.org/0000-0002-4571-2306
D. T. Frayer https://orcid.org/0000-0003-1924-1122
A.-L. Tsai https://orcid.org/0000-0002-3211-4219
K. Rowlands https://orcid.org/0000-0001-7883-8434
T. T. Takeuchi https://orcid.org/0000-0001-8416-7673
A. Leśniewska https://orcid.org/0000-0001-8723-3533
M. P. Koprowski https://orcid.org/0000-0001-5785-1154
J. Nadolny https://orcid.org/0000-0003-1440-9061
M. Solar https://orcid.org/0000-0002-3148-1359
J. Zavala https://orcid.org/0000-0002-7051-1100
P. Bartczak https://orcid.org/0000-0002-3466-3190

References

Alatalo, K., Blitz, L., Young, L. M., et al. 2011, ApJ, 735, 88
Alatalo, K., Crocker, A. F., Aalto, S., et al. 2015a, MNRAS, 450, 3874
Alatalo, K., Davis, T. A., Bureau, M., et al. 2013, MNRAS, 432, 1796
Alatalo, K., Lacy, M., Lanz, L., et al. 2015b, ApJ, 798, 31
Alatalo, K., Lisenfeld, U., Lanz, L., et al. 2016, ApJ, 827, 106
Ali, A., Amer, M. A., Dopita, M. A., Vogt, F. P. A., & Basurah, H. M. 2015, A&A, 583, A83
Ali, A., & Dopita, M. A. 2019, MNRAS, 484, 3251
Andersen, P., & Hjorth, J. 2018, MNRAS, 480, 68
Ashley, T., Marcum, P. M., Alpaslan, M., Fanelli, M. N., & Frost, J. D. 2019, AJ, 157, 158
Ashley, T., Marcum, P. M., & Fanelli, M. N. 2017, AJ, 153, 158
Ashley, T., Marcum, P. M., & Fanelli, M. N. 2018, AJ, 155, 15
Babyk, I. V., McNamara, B. R., Tamhane, P. D., et al. 2019, ApJ, 887, 149
Baldry, I. K., Robotham, A. S. G., Hill, D. T., et al. 2010, MNRAS, 404, 86
Barrera-Ballesteros, J. K., Falcón-Barroso, J., García-Lorenzo, B., et al. 2014, A&A, 568, A70
Barrera-Ballesteros, J. K., García-Lorenzo, B., Falcón-Barroso, J., et al. 2015, A&A, 582, A21
Bassett, R., Bekki, K., Cortese, L., et al. 2017, MNRAS, 470, 1991
Bekki, K. 2014, MNRAS, 438, 444
Bendo, G. J., Galliano, F., & Madden, S. C. 2012, MNRAS, 423, 197
Bezanson, R., Spilker, J. S., Suess, K. A., et al. 2022, ApJ, 925, 153
Binette, L., Magris, C. G., Stasińska, G., & Bruzual, A. G. 1994, A&A, 292, 13
Bisbas, T. G., Papadopoulos, P. P., & Viti, S. 2015, ApJ, 803, 37
Bisbas, T. G., van Dishoeck, E. F., Papadopoulos, P. P., et al. 2017, ApJ, 839, 90
Bitsakis, T., Sánchez, S. F., Ciesla, L., et al. 2019, MNRAS, 483, 370
Bluck, A. F. L., Maiolino, R., Piotrowska, J. M., et al. 2020a, MNRAS, 499, 230
Bluck, A. F. L., Maiolino, R., Sánchez, S. F., et al. 2020b, MNRAS, 492, 96
Bluck, A. F. L., Mendel, J. T., Ellison, S. L., et al. 2014, MNRAS, 441, 599
Bluck, A. F. L., Mendel, J. T., Ellison, S. L., et al. 2016, MNRAS, 462, 2559
Bocchio, M., Micelotta, E. R., Gautier, A. L., & Jones, A. P. 2012, A&A, 545, A124
Bohigas, J., Escalante, V., Rodríguez, M., & Dufour, R. J. 2015, MNRAS, 447, 817
Bolatto, A. D., Warren, S. R., Leroy, A. K., et al. 2013, Natur, 499, 450
Boselli, A., Cortese, L., & Boquien, M. 2014, A&A, 564, A65
Boselli, A., Eales, S., Cortese, L., et al. 2010, PASP, 122, 261
Bravo, M., Robotham, A. S. G., Lagos, C. d. P., et al. 2023, MNRAS, 522, 4481
Brownson, S., Belfiore, F., Maiolino, R., Lin, L., & Carniani, S. 2020, MNRAS Lett., 498, L66
Brüggen, M., & Scannapieco, E. 2020, ApJ, 905, 19
Bryant, J. J., Croom, S. M., van de Sande, J., et al. 2019, MNRAS, 483, 458
Burgarella, D., Nanni, A., Hirashita, H., et al. 2020, A&A, 637, A32
Byrne, L., Faucher-Giguère, C. A., Wellons, S., et al. 2023, arXiv:2310.16086
Calura, F., Pozzi, F., Cresci, G., et al. 2017, MNRAS, 465, 54
Cao, X., Chen, Y. M., Shi, Y., et al. 2022, NatAs, 6, 1464
Carter, M., Lazareff, B., Maier, D., et al. 2012, A&A, 538, A89
Ceverino, D., & Klypin, A. 2009, ApJ, 695, 292
Chabrier, G. 2003, ApJL, 586, L133
Chan, T. K., Kereš, D., Hopkins, P. F., et al. 2019, MNRAS, 488, 3716
Cheung, E., Bundy, K., Cappellari, M., et al. 2016, Natur, 533, 504
Cicone, C., Maiolino, R., Sturm, E., et al. 2014, A&A, 562, A21
Cid Fernandes, R., Stasińska, G., Mateus, A., & Vale Asari, N. 2011, MNRAS, 413, 1687
Cid Fernandes, R., Stasińska, G., Schlickmann, M. S., et al. 2010, MNRAS, 403, 1036
Ciesla, L., Boquien, M., Boselli, A., et al. 2014, A&A, 565, A128
Ciesla, L., Boselli, A., Smith, M. W. L., et al. 2012, A&A, 543, A161
Clark, C. J. R., Dunne, L., Gomez, H. L., et al. 2015, MNRAS, 452, 397
Conroy, C., Graves, G. J., & van Dokkum, P. G. 2014, ApJ, 780, 33
Conroy, C., van Dokkum, P. G., & Kravtsov, A. 2015, ApJ, 803, 77
Cormier, D., Madden, S. C., Lebouteiller, V., et al. 2014, A&A, 564, A121
Cortese, L., Boissier, S., Boselli, A., et al. 2012a, A&A, 544, A101
Cortese, L., Ciesla, L., Boselli, A., et al. 2012b, A&A, 540, A52
Cortese, L., Fritz, J., Bianchi, S., et al. 2014, MNRAS, 440, 942
Cuisinier, F., Acker, A., & Koeppen, J. 1996, A&A, 307, 215
Dalla Vecchia, C., & Schaye, J. 2012, MNRAS, 426, 140
Davé, R., Anglés-Alcázar, D., Narayanan, D., et al. 2019, MNRAS, 486, 2827
Davies, L. J. M., Robotham, A. S. G., Driver, S. P., et al. 2015, MNRAS, 452, 616
Davies, L. J. M., Robotham, A. S. G., Lagos, C. d. P., et al. 2019, MNRAS, 483, 5444
Davis, T. A., Alatalo, K., Sarzi, M., et al. 2011, MNRAS, 417, 882
Davis, T. A., & Bureau, M. 2016, MNRAS, 457, 272
Davis, T. A., Greene, J., Ma, C. P., et al. 2016, MNRAS, 455, 214
Davis, T. A., Greene, J. E., Ma, C. P., et al. 2019a, MNRAS, 486, 1404
Davis, T. A., Rowlands, K., Allison, J. R., et al. 2015, MNRAS, 449, 3503
Davis, T. A., van de Voort, F., Rowlands, K., et al. 2019b, MNRAS, 484, 2447
Davis, T. A., & Young, L. M. 2019, MNRAS Lett., 489, L108
Davis, T. A., Young, L. M., Crocker, A. F., et al. 2014, MNRAS, 444, 3427
De Vis, P., Dunne, L., Maddox, S., et al. 2017a, MNRAS, 464, 4680
De Vis, P., Gomez, H. L., Schofield, S. P., et al. 2017b, MNRAS, 471, 1743
De Vis, P., Jones, A., Viaene, S., et al. 2019, A&A, 623, A5
Dekel, A., & Silk, J. 1986, ApJ, 303, 39
Devereux, N. A., & Young, J. S. 1990, ApJ, 359, 42
Di Matteo, T., Springel, V., & Hernquist, L. 2005, Natur, 433, 604
di Serego Alighieri, S., Bianchi, S., Pappalardo, C., et al. 2013, A&A, 552, A8
Donevski, D., Damjanov, I., Nanni, A., et al. 2023, A&A, 678, A35
Donevski, D., Lapi, A., Małek, K., et al. 2020, A&A, 644, A144
Draine, B. T., & Salpeter, E. E. 1979, ApJ, 231, 438
Driver, S. P., Hill, D. T., Kelvin, L. S., et al. 2011, MNRAS, 413, 971
Driver, S. P., Wright, A. H., Andrews, S. K., et al. 2016, MNRAS, 455, 3911
Dwek, E., & Arendt, R. G. 1992, ARA&A, 30, 11
Dwek, E., & Cherchneff, I. 2011, ApJ, 727, 63
Dwek, E., Galliano, F., & Jones, A. P. 2007, ApJ, 662, 927
Eales, S., Dunne, L., Clements, D., et al. 2010, PASP, 122, 499
Ellison, S. L., Catinella, B., & Cortese, L. 2018, MNRAS, 478, 3447
Fabian, A. C. 2012, ARA&A, 50, 455
Federrath, C., & Klessen, R. S. 2012, ApJ, 761, 156
Ferrarotti, A. S., & Gail, H. P. 2006, A&A, 447, 553
Ferrière, K. M. 2001, RvMP, 73, 1031

Feruglio, C., Fiore, F., Carniani, S., et al. 2015, A&A, 583, A99
Feruglio, C., Maiolino, R., Piconcelli, E., et al. 2010, A&A, 518, L155
Flores-Fajardo, N., Morisset, C., Stasińska, G., & Binette, L. 2011, MNRAS, 415, 2182
Fluetsch, A., Maiolino, R., Carniani, S., et al. 2019, MNRAS, 483, 4586
French, K. D., Smercina, A., Rowlands, K., et al. 2023, ApJ, 942, 25
French, K. D., Yang, Y., Zabludoff, A., et al. 2015, ApJ, 801, 1
French, K. D., Yang, Y., Zabludoff, A. I., & Tremonti, C. A. 2018a, ApJ, 862, 2
French, K. D., Zabludoff, A. I., Yoon, I., et al. 2018b, ApJ, 861, 123
Furlong, M., Bower, R. G., Crain, R. A., et al. 2017, MNRAS, 465, 722
Gabici, S. 2022, A&ARv, 30, 4
Galametz, M., Madden, S. C., Galliano, F., et al. 2011, A&A, 532, A56
Gall, C., Andersen, A. C., & Hjorth, J. 2011a, A&A, 528, A13
Gall, C., Andersen, A. C., & Hjorth, J. 2011b, A&A, 528, A14
Gall, C., Hjorth, J., & Andersen, A. C. 2011c, A&ARv, 19, 43
Galliano, F., Nersesian, A., Bianchi, S., et al. 2021, A&A, 649, A18
Garcia-Munoz, M., Mason, G. M., & Simpson, J. A. 1975, ApJL, 201, L141
Garcia-Munoz, M., Mason, G. M., & Simpson, J. A. 1977, ApJ, 217, 859
Geach, J. E., Bower, R. G., Alexander, D. M., et al. 2014a, ApJ, 793, 22
Geach, J. E., Hickox, R. C., Diamond-Stanic, A. M., et al. 2014b, Natur, 516, 68
Gensior, J., Kruijssen, J. M. D., & Keller, B. W. 2020, MNRAS, 495, 199
Gobat, R., Daddi, E., Béthermin, M., et al. 2015, A&A, 581, A56
Gobat, R., Magdis, G., D'Eugenio, C., & Valentino, F. 2020, A&A, 644, L7
Gomes, J. M., Papaderos, P., Kehrig, C., et al. 2016, A&A, 588, A68
Gordon, Y. A., Owers, M. S., Pimbblet, K. A., et al. 2017, MNRAS, 465, 2671
Griffith, E., Martini, P., & Conroy, C. 2019, MNRAS, 484, 562
Grossi, M., Corbelli, E., Bizzocchi, L., et al. 2016, A&A, 590, A27
Grossi, M., Hunt, L. K., Madden, S., et al. 2010, A&A, 518, L52
Grossi, M., Hunt, L. K., Madden, S. C., et al. 2015, A&A, 574, A126
Hayakawa, S., Nishimura, S., & Takayanagi, T. 1961, PASJ, 13, 184
Heckman, T. M., Kauffmann, G., Brinchmann, J., et al. 2004, ApJ, 613, 109
Henriques, B. M. B., Yates, R. M., Fu, J., et al. 2020, MNRAS, 491, 5795
Herpich, F., Stasińska, G., Mateus, A., Vale Asari, N., & Cid Fernandes, R. 2018, MNRAS, 481, 1774
Hickox, R. C., Mullaney, J. R., Alexander, D. M., et al. 2014, ApJ, 782, 9
Hill, D. T., Kelvin, L. S., Driver, S. P., et al. 2011, MNRAS, 412, 765
Hirashita, H., & Nozawa, T. 2017, P&SS, 149, 45
Hirashita, H., Nozawa, T., Villaume, A., & Srinivasan, S. 2015, MNRAS, 454, 1620
Hjorth, J., Gall, C., & Michałowski, M. J. 2014, ApJL, 782, L23
Hopkins, P. F., Bundy, K., Hernquist, L., Wuyts, S., & Cox, T. J. 2010, MNRAS, 401, 1099
Hopkins, P. F., Chan, T. K., Ji, S., et al. 2021a, MNRAS, 501, 3640
Hopkins, P. F., Chan, T. K., Squire, J., et al. 2021b, MNRAS, 501, 3663
Hopkins, P. F., Torrey, P., Faucher-Giguère, C. A., Quataert, E., & Murray, N. 2016, MNRAS, 458, 816
Hopkins, P. F., Wetzel, A., Keres, D., et al. 2018a, MNRAS, 477, 1578
Hopkins, P. F., Wetzel, A., Keres, D., et al. 2018b, MNRAS, 480, 800
Hunt, L. K., García-Burillo, S., Casasola, V., et al. 2015, A&A, 583, A114
Hunt, L. K., Testi, L., Casasola, V., et al. 2014, A&A, 561, A49
Hunt, L. K., Weiß, A., Henkel, C., et al. 2017, A&A, 606, A99
Ibar, E., Ivison, R. J., Best, P. N., et al. 2010, MNRAS Lett., 401, L53
Indriolo, N., Fields, B. D., & McCall, B. J. 2009, ApJ, 694, 257
Jin, Y., Chen, Y., Shi, Y., et al. 2016, MNRAS, 463, 913
Jokipii, J. R. 1976, ApJ, 208, 900
Jokipii, J. R., & Parker, E. N. 1969, ApJ, 155, 799
Jones, A. P. 2004, in ASP Conf. Ser. 309, Astrophysics of Dust, ed. A. N. Witt, G. C. Clayton, & B. T. Draine (San Francisco, CA: ASP), 347
Jones, A. P., Tielens, A. G. G. M., Hollenbach, D. J., & McKee, C. F. 1994, ApJ, 433, 797
Joye, W. A., & Mandel, E. 2003, in ASP Conf. Ser. 295, Astronomical Data Analysis Software and Systems XII, ed. H. E. Payne, R. I. Jedrzejewski, & R. N. Hook (San Francisco, CA: ASP), 489
Kehrig, C., Monreal-Ibero, A., Papaderos, P., et al. 2012, A&A, 540, A11
Kennicutt, R. C., Jr. 1998, ApJ, 498, 541
Khokhlov, A., Mueller, E., & Hoeflich, P. 1993, A&A, 270, 223
Kim, D. W., James, N., Fabbiano, G., Forbes, D., & Alabi, A. 2019, MNRAS, 488, 1072
Kipper, R., Tamm, A., Tempel, E., de Propris, R., & Ganeshaiah Veena, P. 2021, A&A, 647, A32
Knapp, G. R., Gunn, J. E., & Wynn-Williams, C. G. 1992, ApJ, 399, 76
Kokusho, T., Kaneda, H., Bureau, M., et al. 2017, A&A, 605, A74
Kokusho, T., Kaneda, H., Bureau, M., et al. 2019, A&A, 622, A87
Lagos, C. D. P., Davis, T. A., Lacey, C. G., et al. 2014, MNRAS, 443, 1002
Lagos, C. D. P., Padilla, N. D., Davis, T. A., et al. 2015, MNRAS, 448, 1271
Lee, Y. H., Hwang, H. S., Hwang, N., Lee, J. C., & Kim, K. B. 2023, ApJ, 953, 88
Lemson, G. & the Virgo Consortium 2006, arXiv:astro-ph/0608019
Leroy, A. K., Bolatto, A., Gordon, K., et al. 2011, ApJ, 737, 12
Leśniewska, A., & Michałowski, M. J. 2019, A&A, 624, L13
Leśniewska, A., Michałowski, M. J., Gall, C., et al. 2023, ApJ, 953, 27
Li, M., Li, Y., Bryan, G. L., Ostriker, E. C., & Quataert, E. 2020, ApJ, 898, 23
Li, Z., French, K. D., Zabludoff, A. I., & Ho, L. C. 2019, ApJ, 879, 131
Lianou, S., Xilouris, E., Madden, S. C., & Barmby, P. 2016, MNRAS, 461, 2856
Lin, L., Ellison, S. L., Pan, H. A., et al. 2022, ApJ, 926, 175
Lin, L., Hsieh, B. C., Pan, H. A., et al. 2019, ApJ, 872, 50
Liu, D., Schinnerer, E., Groves, B., et al. 2019, ApJ, 887, 235
Luo, Y., Rowlands, K., Alatalo, K., et al. 2022, ApJ, 938, 63
Magdis, G. E., Gobat, R., Valentino, F., et al. 2021, A&A, 647, A33
Maiolino, R., Russell, H. R., Fabian, A. C., et al. 2017, Natur, 544, 202
Martig, M., Bournaud, F., Teyssier, R., & Dekel, A. 2009, ApJ, 707, 250
Martig, M., Crocker, A. F., Bournaud, F., et al. 2013, MNRAS, 432, 1914
Mathews, W. G., & Brighenti, F. 2003, ARA&A, 41, 191
Matthews, L. D., Gérard, E., & Le Bertre, T. 2015, MNRAS, 449, 220
McDermid, R. M., Alatalo, K., Blitz, L., et al. 2015, MNRAS, 448, 3484
McGee, S. L., Balogh, M. L., Wilman, D. J., et al. 2011, MNRAS, 413, 996
Micelotta, E. R., Jones, A. P., & Tielens, A. G. G. M. 2010, A&A, 510, A37
Michałowski, M. J. 2015, A&A, 577, A80
Michałowski, M. J., Gentile, G., Hjorth, J., et al. 2015, A&A, 582, A78
Michałowski, M. J., Hjorth, J., Gall, C., et al. 2019, A&A, 632, A43
Michałowski, M. J., Karska, A., Rizzo, J. R., et al. 2018, A&A, 617, A143
Michałowski, M. J., Murphy, E. J., Hjorth, J., et al. 2010a, A&A, 522, A15
Michałowski, M. J., Watson, D., & Hjorth, J. 2010b, ApJ, 712, 942
Milingo, J. B., Henry, R. B. C., & Kwitter, K. B. 2002, ApJS, 138, 285
Morgan, H. L., & Edmunds, M. G. 2003, MNRAS, 343, 427
Morganti, R., Oosterloo, T., Oonk, J. B. R., Frieswijk, W., & Tadhunter, C. 2015, A&A, 580, A1
Muratov, A. L., Kereš, D., Faucher-Giguère, C. A., et al. 2015, MNRAS, 454, 2691
Muzzin, A., van der Burg, R. F. J., McGee, S. L., et al. 2014, ApJ, 796, 65
Naab, T., Johansson, P. H., & Ostriker, J. P. 2009, ApJL, 699, L178
Nanni, A., Burgarella, D., Theulé, P., Côté, B., & Hirashita, H. 2020, A&A, 641, A168
Nadolny, J., Michałowski, M. J., Parente, M., et al. 2024, A&A, submitted
Nelson, D., Pillepich, A., Springel, V., et al. 2018, MNRAS, 475, 624
Noirot, G., Sawicki, M., Abraham, R., et al. 2022, MNRAS, 512, 3566
Novak, G. S., Ostriker, J. P., & Ciotti, L. 2011, ApJ, 737, 26
O'Dell, C. R., McCullough, P. R., & Meixner, M. 2004, AJ, 128, 2339
Otter, J. A., Rowlands, K., Alatalo, K., et al. 2022, ApJ, 941, 93
Padoan, P., & Nordlund, A 2002, ApJ, 576, 870
Padovani, M., Ivlev, A. V., Galli, D., et al. 2020, SSRv, 216, 29
Padovani, P., Alexander, D. M., Assef, R. J., et al. 2017, A&ARv, 25, 2
Pagotto, I., Krajnović, D., den Brok, M., et al. 2021, A&A, 649, A63
Papaderos, P., Gomes, J. M., Vílchez, J. M., et al. 2013, A&A, 555, L1
Park, M., Tacchella, S., Nelson, E. J., et al. 2022, MNRAS, 515, 213
Pascale, E., Auld, R., Dariush, A., et al. 2011, MNRAS, 415, 911
Peng, Y., Maiolino, R., & Cochrane, R. 2015, Natur, 521, 192
Perna, M., Arribas, S., Catalán-Torrecilla, C., et al. 2020, A&A, 643, A139
Pety, J. 2005, in SF2A-2005: Semaine de l'Astrophysique Francaise, ed. F. Casoli et al. (Paris: EdP-Sciences), 721
Piotrowska, J. M., Bluck, A. F. L., Maiolino, R., & Peng, Y. 2022, MNRAS, 512, 1052
Poggianti, B. M., Moretti, A., Gullieuszik, M., et al. 2017, ApJ, 844, 48
Rémy-Ruyer, A., Madden, S. C., Galliano, F., et al. 2014, A&A, 563, A31
Richtler, T., Hilker, M., Arnaboldi, M., & Barbosa, C. E. 2020, A&A, 643, A119
Rigby, E. E., Maddox, S. J., Dunne, L., et al. 2011, MNRAS, 415, 2336
Robotham, A., Driver, S. P., Norberg, P., et al. 2010, PASA, 27, 76
Rowlands, K., Dunne, L., Maddox, S., et al. 2012, MNRAS, 419, 2545
Rowlands, K., Gomez, H. L., Dunne, L., et al. 2014, MNRAS, 441, 1040
Rowlands, K., Wild, V., Nesvadba, N., et al. 2015, MNRAS, 448, 258
Sahai, R., & Chronopoulos, C. K. 2010, ApJL, 711, L53
Saintonge, A., Catinella, B., Tacconi, L. J., et al. 2017, ApJS, 233, 22
Salpeter, E. E. 1955, ApJ, 121, 161
Sansom, A. E., Glass, D. H. W., Bendo, G. J., et al. 2019, MNRAS, 482, 4617
Sargent, M. T., Daddi, E., Béthermin, M., et al. 2014, ApJ, 793, 19
Sarzi, M., Alatalo, K., Blitz, L., et al. 2013, MNRAS, 432, 1845
Sarzi, M., Shields, J. C., Schawinski, K., et al. 2010, MNRAS, 402, 2187
Sazonova, E., Alatalo, K., Rowlands, K., et al. 2021, ApJ, 919, 134

Schawinski, K., Urry, C. M., Simmons, B. D., et al. 2014, MNRAS, 440, 889
Schaye, J., Crain, R. A., Bower, R. G., et al. 2015, MNRAS, 446, 521
Sharpee, B., Zhang, Y., Williams, R., et al. 2007, ApJ, 659, 1265
Singh, R., van de Ven, G., Jahnke, K., et al. 2013, A&A, 558, A43
Smercina, A., Smith, J. D. T., Dale, D. A., et al. 2018, ApJ, 855, 51
Smercina, A., Smith, J. D. T., French, K. D., et al. 2022, ApJ, 929, 154
Smith, D. J. B., Dunne, L., Maddox, S. J., et al. 2011, MNRAS, 416, 857
Smith, M. W. L., Gomez, H. L., Eales, S. A., et al. 2012, ApJ, 748, 123
Socolovsky, M., Almaini, O., Hatch, N. A., et al. 2018, MNRAS, 476, 1242
Solomon, P. M., Downes, D., Radford, S. J. E., & Barrett, J. W. 1997, ApJ, 478, 144
Sparke, L. S., & Gallagher, J. S., III 2006, Galaxies in the Universe (2nd ed.; Cambridge: Cambridge Univ. Press)
Spitzer, L., Jr., & Tomasko, M. G. 1968, ApJ, 152, 971
Springel, V., Di Matteo, T., & Hernquist, L. 2005a, ApJL, 620, L79
Springel, V., White, S. D. M., Jenkins, A., et al. 2005b, Natur, 435, 629
Stasińska, G., Vale Asari, N., Cid Fernandes, R., et al. 2008, MNRAS Lett., 391, L29
Su, Y., Irwin, J. A., White, R. E., III, & Cooper, M. C. 2015, ApJ, 806, 156
Suess, K. A., Bezanson, R., Spilker, J. S., et al. 2017, ApJL, 846, L14
Tacchella, S., Conroy, C., Faber, S. M., et al. 2022, ApJ, 926, 134
Taylor, M. B. 2005, in ASP Conf. Ser. 347, Astronomical Data Analysis Software and Systems XIV, ed. P. Shopbell, M. Britton, & R. Ebert (San Francisco, CA: ASP), 29
Trayford, J. W., Theuns, T., Bower, R. G., et al. 2016, MNRAS, 460, 3925
Trujillo, I., Ferreras, I., & de La Rosa, I. G. 2011, MNRAS, 415, 3903
Trussler, J., Maiolino, R., Maraston, C., et al. 2020, MNRAS, 491, 5406
Tsai, A. L., Matsushita, S., Kong, A. K. H., Matsumoto, H., & Kohno, K. 2012, ApJ, 752, 38
Tsai, A. L., Matsushita, S., Nakanishi, K., et al. 2009, PASJ, 61, 237
van de Voort, F., Davis, T. A., Kereš, D., et al. 2015, MNRAS, 451, 3269
Vogelsberger, M., Genel, S., Springel, V., et al. 2014, MNRAS, 444, 1518
Walter, F., Bolatto, A. D., Leroy, A. K., et al. 2017, ApJ, 835, 265
Walter, F., Weiss, A., & Scoville, N. 2002, ApJL, 580, L21
Walters, D., Woo, J., & Ellison, S. L. 2022, MNRAS, 511, 6126
Whitaker, K. E., Narayanan, D., Williams, C. C., et al. 2021, ApJL, 922, L30
Woodrum, C., Williams, C. C., Rieke, M., et al. 2022, ApJ, 940, 39
Wright, R. J., Lagos, C. D. P., Davies, L. J. M., et al. 2019, MNRAS, 487, 3740
Wu, P. F., Bezanson, R., D'Eugenio, F., et al. 2023, ApJ, 955, 75
Yan, R., & Blanton, M. R. 2012, ApJ, 747, 61
Yanasak, N. E., Wiedenbeck, M. E., Mewaldt, R. A., et al. 2001, ApJ, 563, 768
Yepes, G., Kates, R., Khokhlov, A., & Klypin, A. 1997, MNRAS, 284, 235
Yesuf, H. M., French, K. D., Faber, S. M., & Koo, D. C. 2017, MNRAS, 469, 3015
Yesuf, H. M., & Ho, L. C. 2020, ApJ, 900, 107
Young, L. M., Bureau, M., Davis, T. A., et al. 2011, MNRAS, 414, 940
Young, L. M., Scott, N., Serra, P., et al. 2014, MNRAS, 444, 3408
Zanella, A., Valentino, F., Gallazzi, A., et al. 2023, MNRAS, 524, 923
Zavala, J. A., Casey, C. M., Scoville, N., et al. 2019, ApJ, 887, 183
Zhang, C., Peng, Y., Ho, L. C., et al. 2019, ApJL, 884, L52
Zhou, S., Li, C., Hao, C. N., et al. 2021, ApJ, 916, 38